Inter-comparison of stratospheric O3 and NO2 abundances retrieved from balloon borne direct sun observations and Envisat/SCIAMACHY limb measurements

A. Butz, H. Bösch, C. Camy-Peyret, M. Chipperfield, M. Dorf, G. Dufour, K. Grunow, P. Jeseck, S. Kühl, Sébastien Payen, et al.

Atmos. Chem. Phys., 6, 1293–1314, 2006
www.atmos-chem-phys.net/6/1293/2006/

Atmospheric Chemistry and Physics

Inter-comparison of stratospheric O_3 and NO_2 abundances retrieved from balloon borne direct sun observations and Envisat/SCIAMACHY limb measurements

A. Butz[1,2], H. Bösch[1,*], C. Camy-Peyret[2], M. Chipperfield[5], M. Dorf[1], G. Dufour[2,], K. Grunow[6], P. Jeseck[2], S. Kühl[1], S. Payan[2], I. Pepin[2], J. Pukite[1,7], A. Rozanov[3], C. von Savigny[3], C. Sioris[4], T. Wagner[1], F. Weidner[1], and K. Pfeilsticker[1]**

[1]Institut für Umweltphysik, University of Heidelberg, Heidelberg, Germany
[2]Lab. de Physique Moléculaire pour l'Atmosphère et l'Astrophysique (LPMAA), Univ. Pierre et Marie Curie, Paris, France
[3]Institute of Environmental Physics and Institute of Remote Sensing, University of Bremen, Bremen, Germany
[4]Harvard-Smithsonian Center for Astrophysics, Cambridge, USA
[5]Institute for Atmospheric Science, School of Earth and Environment, University of Leeds, Leeds, UK
[6]Meteorologisches Institut, Freie Universität Berlin, Berlin, Germany
[7]Institute of Atomic Physics and Spectroscopy, University of Latvia, Riga, Latvia
[*]now at: Jet Propulsion Laboratory, California Institute of Technology, Pasadena, USA
[**]now at: Department of Chemistry, University of Waterloo, Ontario, Canada

Received: 15 August 2005 – Published in Atmos. Chem. Phys. Discuss.: 27 October 2005
Revised: 2 February 2006 – Accepted: 24 February 2006 – Published: 24 April 2006

Abstract. Stratospheric O_3 and NO_2 abundances measured by different remote sensing instruments are intercompared: (1) Line-of-sight absorptions and vertical profiles inferred from solar spectra in the ultra-violet (UV), visible and infrared (IR) wavelength ranges measured by the LPMA/DOAS (Limb Profile Monitor of the Atmosphere/Differential Optical Absorption Spectroscopy) balloon payload during balloon ascent/descent and solar occultation are examined with respect to internal consistency. (2) The balloon borne stratospheric profiles of O_3 and NO_2 are compared to collocated space-borne skylight limb observations of the Envisat/SCIAMACHY satellite instrument. The trace gas profiles are retrieved from SCIAMACHY spectra using different algorithms developed at the Universities of Bremen and Heidelberg and at the Harvard-Smithsonian Center for Astrophysics. A comparison scheme is used that accounts for the spatial and temporal mismatch as well as differing photochemical conditions between the balloon and satellite borne measurements. It is found that the balloon borne measurements internally agree to within ±10% and ±20% for O_3 and NO_2, respectively, whereas the agreement with the satellite is ±20% for both gases in the 20 km to 30 km altitude range and in general worse below 20 km.

Correspondence to: A. Butz
(andre.butz@iup.uni-heidelberg.de)

1 Introduction

Stratospheric NO_x (=NO+NO_2) is responsible for up to 70% of the stratospheric O_3 loss (Crutzen, 1970; Portmann et al., 1999). NO_x reactions dominate the catalytic destruction of O_3 between 25 and 40 km altitude via

$$NO + O_3 \longrightarrow NO_2 + O_2 \quad \text{(R1)}$$

$$NO_2 + h \cdot \nu \longrightarrow NO + O \quad \text{(R2)}$$

$$NO_2 + O \longrightarrow NO + O_2. \quad \text{(R3)}$$

Reactions (R1) and (R2), account for more than 90% of NO_x chemistry in the lower stratosphere (Del Negro et al., 1999; Cohen et al., 2000). Thus, NO_2 and O_3 measurements are of primary importance to study the photochemistry of stratospheric O_3. Recent studies by Dufour et al. (2005) indicate that for selected geophysical conditions the agreement between measured and photochemically modeled O_3 and NO_x is better than 10%. Accordingly, high precision measurements are required to constrain or to be compared with photochemical models.

Past observations of these key species involve in-situ as well as optical remote sensing instrumentation operated from ground, aircraft, balloons and satellites, exploiting the fact that O_3 and NO_2 absorb electromagnetic radiation in various wavelength ranges. Pioneering work on monitoring atmospheric O_3 abundances has been conducted by Dobson

Published by Copernicus GmbH on behalf of the European Geosciences Union.

(1957a,b). As far as vertical profiling of trace gases is concerned, historically first the solar occultation technique (e.g. Mauldin et al., 1985; Russell III et al., 1988; Camy-Peyret et al., 1993; Sasano et al., 1993) was applied to the UV/visible and IR spectral ranges and only more recently the satellite-borne UV/visible skylight limb technique became available (e.g. Mount et al., 1984; Rusch et al., 1984; Burrows et al., 1995; von Savigny et al., 2003; Sioris et al., 2003; Rozanov et al., 2005b).

The SCanning Imaging Absorption spectroMeter for Atmospheric CHartographY (SCIAMACHY) instrument onboard the European Envisat satellite is a UV/visible/near-IR spectrometer designed to measure direct and scattered sunlight in various viewing directions (Burrows et al., 1995; Bovensmann et al., 1999). An exciting new feature of SCIAMACHY is to probe the atmosphere in subsequent and spatially overlapping nadir and limb scanning observations. This will eventually allow to discriminate between the measured total atmospheric column amounts (nadir) and total stratospheric columns obtained from integrated stratospheric profiles to yield tropospheric column amounts of the targeted gases (Sioris et al., 2004; Sierk et al., 2006).

Here, we present O_3 and NO_2 stratospheric profiles retrieved from SCIAMACHY skylight limb observations using first retrieval exercises developed at the Universities of Bremen (IUP-Bremen) and Heidelberg (IUP-Heidelberg) and at the Harvard-Smithsonian Center for Astrophysics (Harvard). The present study aims at estimating the accuracy of the inferred vertical profiles of stratospheric O_3 and NO_2 by comparison to the corresponding data retrieved from traditional balloon borne solar occultation measurements performed by the LPMA/DOAS (Limb Profile Monitor of the Atmosphere/Differential Optical Absorption Spectroscopy) balloon payload (Camy-Peyret, 1995; Ferlemann et al., 1998; Harder et al., 1998; Bösch et al., 2003). For ENVISAT validation purposes, LPMA/DOAS has been deployed at different launch locations and in different seasons during the recent past. It allows us to perform simultaneous measurements of targeted gases in various wavelength ranges covering the UV to the IR.

Therefore in a first exercise, the internal consistency of the LPMA/DOAS observations is checked by comparing slant column amounts of O_3 and NO_2 (taken from the balloon to the sun) inferred from the visible and IR spectral ranges. Since instrumental setup and retrieval algorithms are inherently different for the DOAS and LPMA instrument but the line-of-sight is inherently the same, inferred line-of-sight absorptions are compared and discussed with respect to precision and accuracy of the instruments. Further, the vertical profiles are analyzed regarding altitude resolution and implications for satellite validation. In the second part, the balloon borne profiles of O_3 and NO_2 are compared with collocated profiles inferred from SCIAMACHY skylight limb observations. Spatial and temporal coincidences of the balloon and satellite borne measurements are identified using air mass trajectory calculations based on ECMWF analyses. In addition, for the photochemically short-lived NO_2 radical, the diurnal variation is modelled on the calculated air mass trajectory in order to consider the different daylight hour of the satellite and the balloon borne observations. Finally, after accounting for the spatial and temporal mismatch as well as the differing photochemical conditions, the balloon and satellite borne measurements are inter-compared and discussed with respect to inherent errors and possible further improvements of the involved algorithms. A schematic drawing which illustrates the presented comparison and validation strategy is shown in Fig. 1.

2 Methods

2.1 O_3 and NO_2 profiles inferred from LPMA/DOAS observations

Since details on the instrumental setup and performance of the French/German LPMA/DOAS balloon payload have been reported elsewhere (Camy-Peyret, 1995; Ferlemann et al., 1998), only a short description of the instrumental features important for the present study is given here. The payload is mounted on an azimuth-controlled gondola and comprises a sun-tracker (Hawat et al., 1998) and three optical spectrometers which analyze direct sunlight over virtually the entire wavelength range from the UV to the mid-IR. Sunlight is collected by the automated sun-tracker (beam diameter 10 cm), which points to the center of the solar disk within 30 arcsec. It directs the inner core (beam diameter 5 cm) of the solar beam into a Fourier Transform spectrometer (FT-IR) operated by LPMAA (effective field of view FOV$\simeq$0.2°) while two small telescopes (diameter 1 cm each, effective field of view FOV$\simeq$0.53°) mounted into the beam's outer fringe feed the collected sunlight into the two DOAS spectrometers via glass fibre bundles. This optical setup guarantees that the UV/visible (DOAS) and IR (LPMA, FT-IR) spectrometers analyze direct sunlight which traversed almost the same atmospheric air masses, (except for the slightly different effective FOV of both spectrometers). The measurements are performed during balloon ascent/descent and in solar occultation geometry with moderate spectral resolution in the UV/visible (UV: FWHM$\simeq$0.5 nm, visible: FWHM$\simeq$1.5 nm) and high spectral resolution in the IR (apodized resolution $\simeq$0.02 cm^{-1}).

In addition to the spectrometers observing direct sunlight a small versatile UV/visible spectrometer has been operated in limb scattering geometry aboard the same balloon gondola since 2002. The instrumental setup, performance and first results are published in Weidner et al. (2005). The inferred O_3 and NO_2 abundances show overall good agreement with the data inferred from the direct sun measurements.

The retrieval of O_3 and NO_2 profiles from LPMA/DOAS measurements is split in two steps. First the trace gas

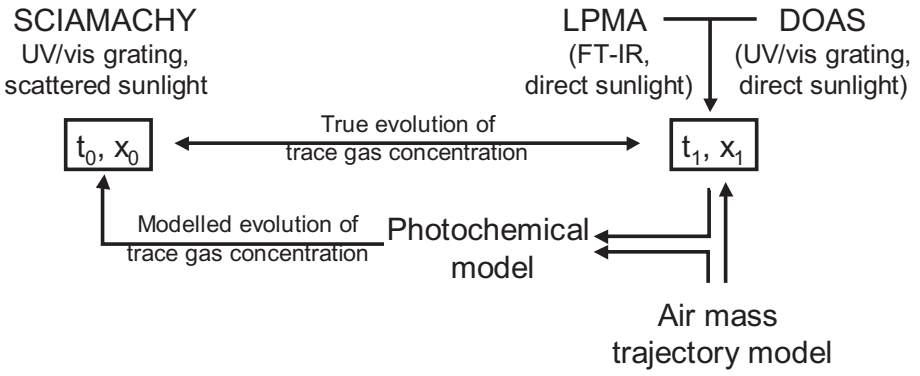

Fig. 1. Schematic drawing of the presented comparison and validation strategy. SCIAMACHY observations are conducted at time t_0 and location x_0. Prior to the balloon flight dedicated to SCIAMACHY validation, the air mass trajectory model is used to optimize the time t_1 and location x_1 of the LPMA/DOAS balloon borne observations, e.g. by optimizing the launch time of the balloon. After the balloon flight, the trajectory model calculates the air mass history in order to identify satellite measurements which actually sampled the same air masses as the balloon borne instruments. In a Lagrangian approach the illumination history of the coincident air masses is fed into a photochemical model to reproduce the evolution of the considered trace gases between satellite and balloon borne observations as realistically as possible. First the balloon borne LPMA and DOAS measurements are checked for internal consistency, then they are compared to SCIAMACHY data accounting for the photochemical history of the sampled air parcels.

concentrations integrated along the line-of-sight (Slant Column Densities (SCDs)) are inferred from individual solar spectra. Then the SCDs are inverted to vertical profiles of the respective trace gases.

2.1.1 DOAS O_3 and NO_2 SCD retrieval

The UV/visible spectra recorded by the two DOAS spectrometers are analyzed for trace gas absorptions applying the DOAS retrieval algorithm (Platt, 1994; Stutz and Platt, 1996). Each spectrum is evaluated with respect to a solar reference spectrum guaranteeing the removal of solar Fraunhofer lines. The solar reference spectrum usually is the spectrum for which the air mass along the line-of-sight and the residual trace gas absorption are minimal. The residual absorption in the solar reference is determined using Langley's extrapolation to zero air mass.

O_3 SCDs are retrieved from the differential structures in the Chappuis absorption band between 545 nm and 615 nm where the temperature and pressure dependence of the O_3 absorption cross section taken from Anderson et al. (1992) is negligible (Burkholder et al., 1994; Orphal, 2003). Remaining trace gas absorptions are dealt with by simultaneously fitting two NO_2 absorption cross sections recorded at T$\simeq$218 K and T$\simeq$238 K in the laboratory, wavelength aligned to cross sections from Voigt et al. (2002) and orthogonalized with respect to each other. Further, an oxygen dimer (O_4) absorption cross section taken from Hermans (2002) and an H_2O absorption cross section generated from HITRAN 2000 (Rothman et al., 2003) by convolution to our spectral resolution are considered. Rayleigh and Mie scattering are accounted for by including a third order polynomial in the fitting procedure. In addition we allow for a first order polynomial which is subtracted from the measured intensity before any algebraic manipulation to correct for instrumental straylight. In the final evaluation the relative wavelength alignment of the absorption cross sections and the solar reference spectrum is fixed and only the measured spectrum is allowed to shift and stretch.

The line-of-sight absorptions of NO_2 are inferred from the 435 nm to 485 nm wavelength range. Interfering absorption features come from O_4 (Hermans, 2002) and O_3. Two O_3 absorption cross sections recorded in the laboratory at T$\simeq$230 K and T$\simeq$244 K, aligned to cross sections from Voigt et al. (2001), are orthogonalized and fitted simultaneously. Broad band spectral features are represented by a fourth order polynomial. Instrumental straylight correction and wavelength alignment are treated as in the case of the O_3 analysis. Additional complications arise from the temperature dependence of the NO_2 absorption cross section while the pressure dependence is negligible at our spectral resolution (Pfeilsticker et al., 1999; Orphal, 2003). The NO_2 analysis is performed using absorption cross sections recorded in our laboratory scaled and aligned to convolved cross sections from Harder et al. (1997) at T=217 K, T=230 K, T=238 K and T=294 K. The resulting four sets of NO_2 SCDs are linearly interpolated to the effective NO_2 concentration weighted temperature along the line-of-sight for each spectrum.

The error bars of the retrieved SCDs are estimated via Gaussian error propagation from the statistical error given by the fitting routine, the error in determining the residual absorber amount in the solar reference spectrum and the errors of the absorption cross sections (1% for O_3, 4% for NO_2). For NO_2 additional errors coming from unaccounted features of the temperature dependence of the absorption cross

section (2%) and from the convolution to our spectral resolution (1%) are taken into account. The statistical error comprises the 1-σ fitting error, errors coming from systematic residual absorption features and from shift and stretch of the fitted spectrum. The error of the residual absorber amount in the solar reference spectrum is dominated by the estimated accuracy (5%) of the overhead air mass. The errors of the retrieved O_3 SCDs are governed by the latter error contribution while, for NO_2, fitting errors become important when NO_2 abundances are very low. In total, typical accuracies of the DOAS O_3 and NO_2 measurements are better than 5% and 10%, respectively.

Typical optical densities range between 10^{-1} and 10^{-3} for both gases. All DOAS data presented in this study originate from spectra in the visible wavelength range. NO_2 SCDs are also retrieved in the 370 nm to 390 nm wavelength range measured by the UV spectrograph. As NO_2 SCDs inferred from the UV and the visible do not differ significantly, only data inferred from the visible spectrograph are shown exhibiting smaller error bars. Evaluating O_3 in the UV is difficult due to the strong temperature dependence and the strong absorption (optical densities $\simeq$1) below 350 nm which renders the DOAS approach questionable (Frankenberg et al., 2005). For further information on the spectral retrieval see Harder et al. (1998, 2000), Ferlemann et al. (1998, 2000), and Bösch et al. (2003).

2.1.2 LPMA O_3 and NO_2 SCD retrieval

The SCD retrieval of O_3, NO_2, NO, HNO_3, N_2O, CH_4, HCl, CO_2 and $ClONO_2$ is performed simultaneously using a multi fit of 6 to 11 micro-windows. The possibility to retrieve all species depends on the actual filters and beamspliters used for the FT-IR measurements. The target micro-windows for O_3 and NO_2 are 3040.03 cm^{-1} to 3040.85 cm^{-1} and 2914.36 cm^{-1} to 2915.16 cm^{-1}, respectively. Typically the O_3 absorption lines in the main target window become saturated during deep solar occultation reducing the sensitivity of the retrieval to changes in O_3 abundances along the line-of-sight. Thus, an additional micro-window between 1818.09 cm^{-1} and 1820.98 cm^{-1} with non-saturated O_3 absorption features is added if available. Interfering absorbers in the O_3 and NO_2 target windows are H_2O, CO_2, NO, CH_4 and H_2O, O_3, CH_4, respectively. Additional information on ozone SCDs comes from weak absorption in the micro-windows dedicated to NO_2 (2914.36–2915.16 cm^{-1}), and CO_2 (1933.89–1940.00 cm^{-1}). For NO_2, weak absorption in the HCl micro-window (2944.71–2945.11 cm^{-1}) improves the SCD retrieval. Based on absorption line parameters from HITRAN 2004 (Rothman et al., 2005) and a reasonable a priori guess for the trace gas profiles, a forward model calculates synthetic spectra which are fitted to the measured ones by a non-linear Levenberg-Marquardt algorithm. The calculation of the synthetic spectra relies on atmospheric parameters taken from nearby radiosonde launches and climatological and meteorological model data. Fitting parameters include a polynomial of up to third order, a zero order wavelength shift and several parameters to adjust the instrumental line shape (ILS). All auxiliar ILS parameters are determined separately in various test runs and finally set to a fixed value for all spectra during a balloon flight.

The error bars comprise the statistical error of the fitting routine (1-σ), the uncertainty in determining the instrumental line shape ($\sim$5%), the error coming from the ambient atmospheric parameters ($<$1%) and their impact on the spectroscopic parameters and the stated error bars of the latter (5% to 10% for O_3, 2% to 5% for NO_2 (Rothman et al., 2005)). In total the systematic contribution to the SCD error is estimated to 10% for both gases. Since the pre-flight alignment and in-flight stability of the LPMA instrument improved during the suite of considered balloon flights between 1996 and 2003, the analysis of earlier balloon flights usually yields larger errors than analysis of the more recent ones. Typical errors of the retrieved O_3 SCDs range between 10% and 15% and are dominated by the accuracies of the spectroscopic parameters and the estimated accuracy of the instrumental line shape function. The errors of the NO_2 SCDs range between 10% and 25%. As in the case of the DOAS error budget, fitting errors become important for NO_2 when its abundances are very low e.g. for the flight from Kiruna in February 1999, where NO_2 SCDs are close to the detection limit of the LPMA instrument. For earlier work on LPMA data see Payan et al. (1998, 1999) and Dufour et al. (2005).

2.1.3 LPMA/DOAS O_3 and NO_2 profile retrieval

Each spectrum yields an O_3 and NO_2 SCD according to the specifications described above. Vertical trace gas profiles are inferred separately from the measurements during balloon ascent and solar occultation. We refer to the respective set of SCDs as the measurement vector $\boldsymbol{y}$. In keeping with the standard notation the true trace gas profile is denoted $\boldsymbol{x}$ (Rodgers, 2000). The forward model which links the measurements and the vertical profile is straight forward to obtain by raytracing the path of the incoming light from the sun to the detector. Assuming a spherical, layered atmosphere including refraction, the elements K_{ij} of the weighting function matrix $\mathbf{K}$ are given by the ratio of the slant path through layer j and the height of layer j for the observation geometry of spectrum i. The inversion problem can be stated in linear form

$$\boldsymbol{y} = \mathbf{K}\boldsymbol{x} + \boldsymbol{\epsilon}, \tag{1}$$

where $\boldsymbol{\epsilon}$ represents the measurement error. A variety of methods exists to invert the weighting function matrix $\mathbf{K}$ and to calculate a retrieved vertical trace gas profile $\hat{\boldsymbol{x}}$ given the measurements $\boldsymbol{y}$. Vertical trace gas profiles from balloon borne measurements shown here are generated using a

linear Maximum A Posteriori inversion algorithm described in Rodgers (2000)

$$\hat{\boldsymbol{x}} = (\mathbf{K}^T \mathbf{S}_\epsilon{}^{-1} \mathbf{K} + \mathbf{S_a}^{-1})^{-1}(\mathbf{K}^T \mathbf{S}_\epsilon{}^{-1} \boldsymbol{y} + \mathbf{S_a}^{-1} \boldsymbol{x_a}), \quad (2)$$

where the superscript T indicates transposed matrices. A priori, $\mathbf{S_a}$, as well as measurement covariance matrices, $\mathbf{S}_\epsilon$, are assumed to be diagonal. The a priori profile $\boldsymbol{x_a}$ is taken from the satellite retrievals described below or from the SLIMCAT chemical transport model (Chipperfield, 1999). Error propagation is handled by calculating the corresponding error covariance matrix $\hat{\mathbf{S}}$ via

$$\hat{\mathbf{S}} = (\mathbf{K}^T \mathbf{S}_\epsilon{}^{-1} \mathbf{K} + \mathbf{S_a}^{-1})^{-1}. \quad (3)$$

The square roots of the variances $\hat{S}_{ii}$ represent the errors attributed to the retrieved trace gas profile $\hat{\boldsymbol{x}}$.

The quality of the retrieval can be characterized by the averaging kernel matrix $\mathbf{A}$ which gives the relation between the true trace gas profile $\boldsymbol{x}$ and the retrieved one $\hat{\boldsymbol{x}}$

$$\hat{\boldsymbol{x}} = \boldsymbol{x_a} + \mathbf{A}\,(\boldsymbol{x} - \boldsymbol{x_a}) + \text{error terms}. \quad (4)$$

For the Maximum A Posteriori retrieval $\mathbf{A}$ is given through

$$\mathbf{A} = \hat{\mathbf{S}}\,\mathbf{K}^T \mathbf{S}_\epsilon{}^{-1} \mathbf{K}. \quad (5)$$

The width of averaging kernels given by the rows of $\mathbf{A}$ is a measure for the altitude resolution of the measurement. As altitude resolution depends on the weighting function matrix $\mathbf{K}$ and measurement error $\mathbf{S}_\epsilon$ the altitude resolution of the retrieved trace gas profiles is different for the three sensors presented in this study. When comparing trace gas profiles the differing altitude resolution can be accounted for by degrading the altitude resolution of the high resolution profile. First, the profile inversion of the high resolution measurement is performed on the same altitude grid as the inversion of the low resolution data set, then the resulting trace gas profile $\hat{\boldsymbol{x}}_{\boldsymbol{h}}$ is smoothed by the averaging kernel matrix of the low resolution measurement $\mathbf{A_l}$. Accordingly, the smoothed trace gas profile $\hat{\boldsymbol{x}}_{\boldsymbol{s}}$ is given by

$$\hat{\boldsymbol{x}}_{\boldsymbol{s}} = \boldsymbol{x_a} + \mathbf{A_l}\,(\hat{\boldsymbol{x}}_{\boldsymbol{h}} - \boldsymbol{x_a}), \quad (6)$$

where $\boldsymbol{x_a}$ is the a priori profile simultaneously used for both retrievals (Connor et al., 1994; Hendrick et al., 2004). Whenever smoothed profiles are shown in this study they are generated according to Eq. (6).

2.2 O_3 and NO_2 profiles inferred from Envisat/ SCIAMACHY limb observations

The SCIAMACHY instrument, which was put into a sun-synchronous orbit onboard the European Envisat satellite on 28 February 2002, is a UV/visible/near-IR spectrometer (220 nm–2380 nm, FWHM: 0.2 nm–1.5 nm) designed to measure either direct sunlight during solar occultation, direct moonlight during lunar occultation or sunlight scattered by the Earth's atmosphere in nadir or limb direction (e.g. Burrows et al., 1995; Bovensmann et al., 1999). In limb scattering mode SCIAMACHY scans the Earth's atmosphere vertically in steps of 3.3 km from the ground to about 100 km tangent height (vertical field of view at tangent point, FOV$\simeq$2.8 km, horizontal field of view at tangent point, FOV$\simeq$110 km). In addition a horizontal scan is performed at each tangent height covering in total about 960 km at the tangent point. Here, results obtained by the LPMA/DOAS balloon payload since 2003 are used to validate SCIAMACHY limb observations.

O_3 and NO_2 profiles are inferred from SCIAMACHY limb measurements using algorithms developed at the university of Bremen (IUP-Bremen). In the case of NO_2, also data retrieved at the Harvard Smithsonian Center for Astrophysics (Harvard) and a limited data set retrieved by the university of Heidelberg (IUP-Heidelberg) are available. To our knowledge no official ESA products are on hand to be compared with the presented data.

2.2.1 IUP-Bremen O_3 retrieval

The stratospheric ozone profiles are derived from SCIAMACHY limb scattering observations with the Stratozone code (version 1.62) using the method described in von Savigny et al. (2005c). The altitude range from about 15–40 km can be covered with this technique with a vertical resolution of about 4 km. The retrieval technique exploits the absorption in the Chappuis bands of ozone using only three discrete wavelengths as described in Flittner et al. (2000). A non-linear optimal estimation (OE) scheme drives the radiative transfer model SCIARAYS (Kaiser and Burrows, 2003), which is run online to calculate weighting functions and to forward-model the limb radiance profiles. The main error sources are incorrect knowledge of the stratospheric aerosol loading, surface albedo, cloud cover, as well as tangent height errors (von Savigny et al., 2005b). The estimated total error between 15 and 35 km is about 8–14%. The SCIAMACHY limb observations are affected by errors in the tangent height information of up to 2.5 km (von Savigny et al., 2005a), particularly before the improvement of the orbit propagator model on-board the Envisat spacecraft in December 2003. Note that tangent height errors of only 500 m lead to errors in the ozone concentrations of up to 10%. For the stratospheric ozone profile retrievals presented here a tangent height offset for each orbit was derived from the limb measurements in the UV-B spectral range prior to the ozone profile retrieval, using the method described in Kaiser et al. (2004). The precision of the tangent height retrieval method is about 200–300 m.

2.2.2 IUP-Bremen NO_2 retrieval

The forward simulations of the SCIAMACHY limb measurements and the calculations of the appropriate weighting functions are performed employing the SCIATRAN radiative

transfer model (Rozanov et al., 2005a,b), assuming cloud free conditions. In spherical mode the SCIATRAN model calculates the limb radiance properly considering the single scattered radiance and using an approximation to account for multiple scattering. Vertical distributions of NO_2 are retrieved from SCIAMACHY limb measurements using the spectral information in the 420–470 nm wavelength interval. To improve the retrieval quality the vertical profiles of O_3 are estimated in combination with NO_2 retrievals using the same spectral information. Limb measurements performed at tangent heights from 12 to 40 km are considered. To reduce the impact of the Fraunhofer structure and incorrect instrument calibration all selected limb scans are divided by the reference limb measurement obtained at a tangent height of about 43 km. To account for broadband features resulting from unknown scattering properties of the atmosphere as well as instrument calibration issues, a cubic polynomial is subtracted from all spectral ratios. The temperature dependent absorption cross sections of O_3 and NO_2 measured by the SCIAMACHY PFM Satellite Spectrometer are used in the forward model (Bogumil et al., 1999). Pressure and temperature profiles are taken from the corresponding ECMWF data. The SCIAMACHY pointing errors are accounted for by applying appropriate tangent height corrections obtained using the TRUE retrievals (Kaiser et al., 2004). The retrieval is performed as described in Rozanov et al. (2005b) using a two-step retrieval procedure. During the preprocessing step which is done for each tangent height independently a possible misalignment of the wavelength grids of the limb spectra, of the reference spectrum and of the forward model is accounted for. Additionally, known corrections, namely, undersampling, Ring spectrum, stray light correction and instrument calibration functions, are applied. The main retrieval step is based on the solution of Eq. (1) employing the optimal estimation technique. Different from the description given in Sect. 2.1.3, the measurement vector $\boldsymbol{y}$ contains the differences between ratios of simulated and measured differential limb spectra at all tangent heights selected for the retrieval with all corrections from the preprocessing step applied. The state vector $\boldsymbol{x}$ contains relative differences of trace gas number densities (with respect to a priori values) at all altitude layers for all gases to be retrieved. The final solution is found employing the information operator approach (Hoogen et al., 1999; Rozanov, 2001) which ensures an additional noise filtering, resulting in more stable profiles.

2.2.3 Harvard NO_2 retrieval

The Harvard-SAO algorithm is described in Sioris et al. (2004) and references therein. Cloud top height is retrieved from channel 6 and is used to define the lower limit of the retrieval. Tangent height (TH) registration is determined by the multi-wavelength ~305 nm knee method (Sioris et al., 2003). The calculated orbital median TH offset is applied to all limb scans if greater than the orbital standard deviation of the TH offsets. The NO_2 fitting window consists of 256 pixels in the 434–495 nm range and the simulations are performed at SCIAMACHY channel 3 spectral resolution (0.5 nm), leading to 114 wavelengths in the same fitting window. The analysis uses a classic two-step approach: spectral fitting followed by inversion of SCDs to a number density profile. The reference spectrum is the co-addition of all spectra between the retrieval upper altitude limit (~40 km) and 70 km. Absorption cross sections included in the fitting process are NO_2 and O_3 from Bogumil et al. (2003), and the collisional oxygen dimer (O_4) from Greenblatt et al. (1990). The temperature dependence of the NO_2 and O_3 absorption cross section is handled by performing three runs with absorption cross sections corresponding to T=203 K, T=223 K, T=243 K (Bogumil et al., 2003). At each tangent height the run which exhibits the smallest errors is chosen for profile retrieval. The inversion of the SCDs to number densitiy profiles is direct, thus a priori is not required in the retrieval range.

2.2.4 IUP-Heidelberg NO_2 retrieval

The IUP-Heidelberg uses a two step approach to retrieve NO_2 vertical profiles from SCIAMACHY limb spectra (Kühl, 2005), see also Krecl et al. (2005) and Haley et al. (2004). First, the SCD of the considered absorber is deduced by Differential Optical Absorption Spectroscopy (Platt, 1994). In the second step the SCDs for the different tangent heights are inverted to concentration profiles by an optimal estimation method (Rodgers, 2000). The DOAS retrieval for NO_2 is performed in the 420–450 nm spectral range. The measured and calibrated spectral information from SCIAMACHY is analyzed with respect to a pseudo top-of-the-atmosphere (TOA) reference spectrum taken as average of SCIAMACHY measurements at tangent heights between 40 to 46 km to infer the SCDs. Considered trace gas absorption cross sections are NO_2 at 223 K from Bogumil et al. (2003), O_3 at 241 K from Bogumil et al. (2003), H_2O at 273 K from Rothman et al. (2003), O_4 at 298 K from Greenblatt et al. (1990). In addition we account for the Ring effect (Grainger and Ring, 1962), instrumental straylight and broadband spectral features by considering a calculated Ring spectrum and the inverse of the TOA reference as fitting parameters. The vertical trace gas profiles are obtained using the same approach as in the case of the balloon borne retrieval, see Sect. 2.1.3. The weighting function matrix $\mathbf{K}$ is calculated by the fully spherical 3-dimensional Monte Carlo radiative transfer model "Tracy" (von Friedeburg, 2003; Weidner et al., 2005), assuming a cloud cover at 10 km altitude. Sensitivity studies show that the impact of clouds on the retrieval of stratospheric NO_2 is negligible. Using the maximum a posteriori technique the vertical trace gas profile is inferred from Eq. (2), where the measurement vector $\boldsymbol{y}$ represents the measured SCDs and the vector $\hat{\boldsymbol{x}}$ the retrieved profile. Our studies show the possibility to retrieve information about the NO_2 concentration in the altitude range from

approximately 15 km to 40 km where averaging kernels are larger than 0.7. The accuracy in this altitude range is approximately 15–25%. Tangent height corrections are performed according to the monthly averaged SCIAMACHY pointing errors given in von Savigny et al. (2005a).

2.3 Air mass trajectory modelling

Balloon borne measurements exhibit several inherent constraints with respect to the time and location of the balloon launch. Balloon launches are possible at a few sites around the world, only. The launching possibility depends on the local surface weather conditions and the balloon's trajectory is determined by the tropospheric and stratospheric wind fields. Furthermore, the LPMA/DOAS payload is supposed to be launched temporally close to local sunset or sunrise as LPMA/DOAS performs measurements during solar occultation. In practise, these constraints make it difficult to get a direct temporal and spatial coincidence with individual satellite measurements such as SCIAMACHY limb observations. In part, the use of air mass trajectory models can help to overcome the shortcomings in balloon borne satellite validation (Bacmeister et al., 1999; Lu et al., 2000; Danilin et al., 2002a,b).

For that purpose, an air mass trajectory model is applied within the framework of Envisat/SCIAMACHY validation (Langematz et al., 1987; Reimer and Kaupp, 1997). It uses the operational ECMWF analyses and forecasts given every 6 h on a $2.5^\circ \times 2.5^\circ$ latitude/longitude grid. Forward and backward trajectories are calculated on isentropic levels from the surface up to 1600 K with interpolation between the levels. The internal time step is 10 minutes and the diabatic and climatological heating rates are based on Newtonian cooling. The results (trajectory points) are stored for each hour.

Backward and forward trajectories start at the balloon measurement locations. For the remote-sensing payload LPMA/DOAS these starting points are the balloon location and the tangent points for balloon ascent and solar occultation, respectively. For post-flight analysis air mass trajectories are calculated for up to 10 days forward and backward in time, but for balloon flight planning purposes the time range is limited by the available ECMWF forecasts: the latest analysis is from 12:00 UT the day before, forecasts are available every 6 h up to 72 h into the future.

The actual geolocations of Envisat/SCIAMACHY observations are provided by the SCIAMACHY Operational Support Team (SOST) through its website (http://atmos.af.op.dlr.de/projects/scops/). For each Envisat orbit, overpass time, geolocation and detailed measurement specifications (e.g. swath, measurement duration, ground pixel size) can be downloaded. For the air mass trajectory based matching technique only the area covered by the tangent points of SCIAMACHY limb is considered. This information is used to find satellite measurement points along the individual air mass trajectories, for which the spatial and temporal mismatch is as small as possible. The match criteria are chosen based on the experience of the ozone Match experiment (von der Gathen et al., 1995). The maximum time mismatch between the satellite observation and the air mass trajectory started at the balloon observation is one hour and the maximum area mismatch is 500 km with respect to the center of the SCIAMACHY limb ground pixel. In case, no Envisat/SCIAMACHY observation satisfies these limits, the distance criterion is weakened to a maximum spatial mismatch of 1000 km.

2.4 Photochemical modelling

On timescales important for this study, i.e. the time between satellite and correlative balloon borne measurement ($<$1 day), the photochemical variation of O_3 is found negligible. Hence, we focus our modelling on the photochemical variation of NO_2. For the impact of the photochemistry of NO_2 on solar occultation measurements and validation studies see also Kerr et al. (1977), Roscoe and Pyle (1987) and Bracher et al. (2005). We use output from a simulation of the SLIMCAT 3-D off-line chemical transport model (CTM) (Chipperfield, 1999) to initialize a 1-D chemistry model of the stratosphere. SLIMCAT output of run 323 is saved at 00:00 UT every 2 days interpolated to the launching sites of the balloon flights. Both photochemical models include a comprehensive set of the relevant gas-phase and heterogenous reactions as given by the JPL-2002 report on Chemical Kinetics and Photochemical Data (Sander et al., 2003). The 1-D chemistry model is an updated version of the model used in Bösch et al. (2003). Stratospheric chemistry is modelled on 19 potential temperature (Θ) levels between Θ=336 K ($\simeq$11 km) and Θ=1520 K ($\simeq$42 km). Aerosol loadings are taken from Deshler et al. (2003) as recommended by Dufour et al. (2005). Photolysis rates are interpolated with respect to pressure, temperature, overhead ozone and solar zenith angle (SZA) from a lookup table where the actinic fluxes are calculated as recommended by Lary and Pyle (1991) and validated for J_{NO_2} by Bösch et al. (2001).

If available the 1-D model is initialized at 00:00 UT with SLIMCAT output of the same day at the balloon launch site. If output is not available on the day of the balloon flight, we decide whether to take output from the day before or after the flight by comparing the measured O_3, NO_2 and if available CH_4 and N_2O profiles to the modelled ones and choosing the output which produces better agreement with the measurement. While the model is run with fixed pressures and temperatures for each Θ level taken from the meteorological support data of the balloon flight, the SZA timeline is taken from the air mass trajectory calculations to guarantee that the photochemical evolution of the modelled air mass corresponds to the true evolution between initialization of the model, satellite measurement and balloon borne observation. For simplicity a single representative SZA timeline is chosen for all Θ levels. In addition O_3, NO_2, NO and N_2O_5

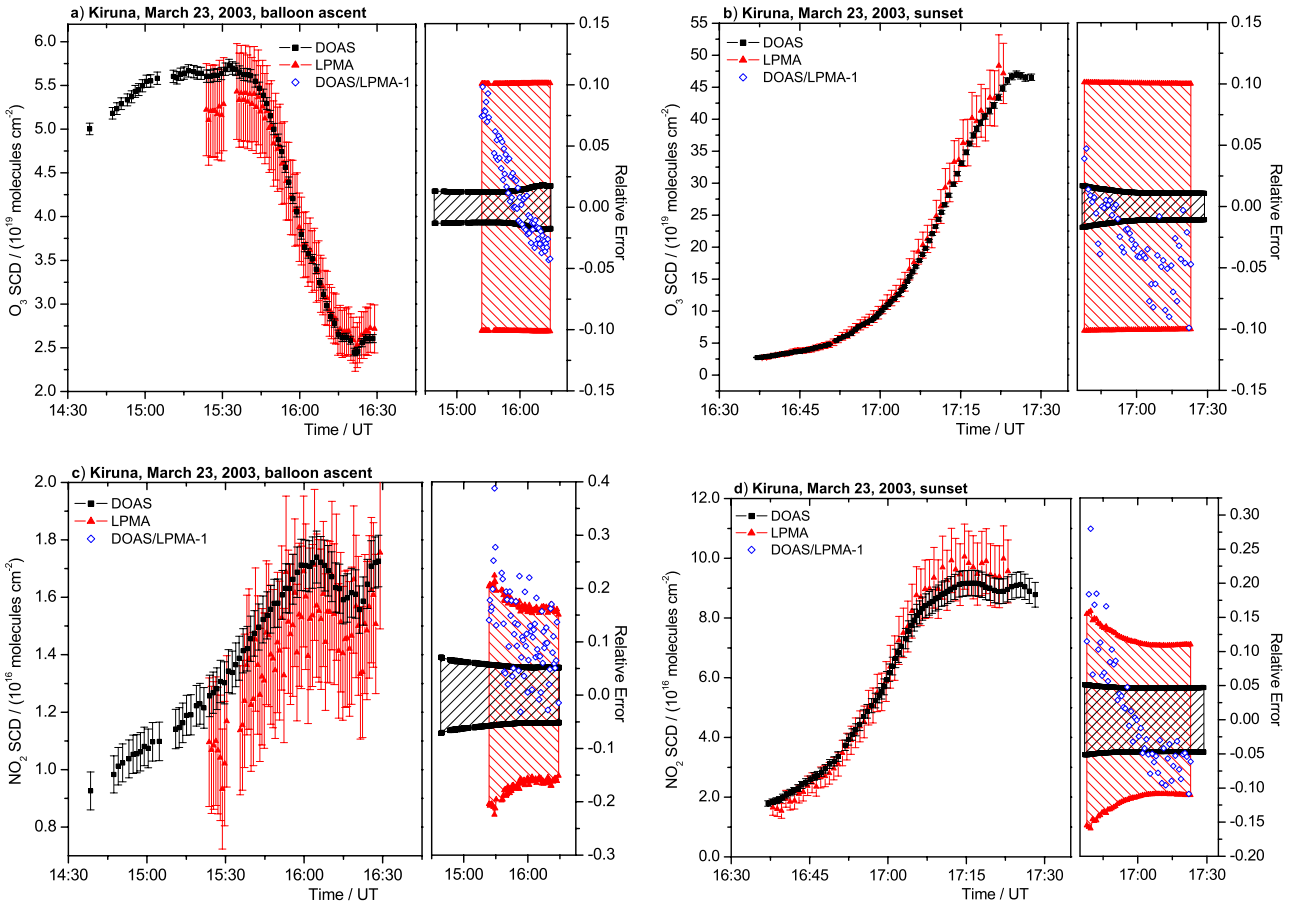

Fig. 2. Slant Column Densities of O_3 (panels **a** and **b**) and NO_2 (panels **c** and **d**) retrieved from LPMA (red triangles) and DOAS (black boxes) direct solar spectra measured at Kiruna on 23 March 2003, during balloon ascent (panels a and c) and sunset (panels b and d). Each panel consists of two sub-panels showing the measured SCDs on the left and the corresponding relative errors and deviations (blue open stars), i.e. SCD(DOAS) / SCD(LPMA) - 1, on the right. For clarity not all DOAS data points are shown.

are scaled at initialization in a way that the model can reproduce the balloon borne O_3 and NO_2 profiles in the evening (Bracher et al., 2005).

In general, each spectrum measured by SCIAMACHY as well as by the balloon borne instruments is a composite of several photochemical conditions since the SZA varies along the line-of-sight through the atmosphere. All satellite measurements presented here are conducted in the morning far from sunset or sunrise where the photochemical variation of NO_2 is weak. Hence, we assume a fixed SZA for the SCIAMACHY observations. However, the time-lag to the validation measurements is on the order of several hours and balloon borne profiles are inferred from measurements close to sunset when the photochemical variation of NO_2 is strongest. Introducing the photochemical weighting factors κ_{kj}, balloon observations are scaled to the photochemical conditions of the satellite measurements. Given the model data along the SZA timeline of a given air mass trajectory, κ_{kj} is defined by

$$\kappa_{kj} = \frac{a_{kj}}{b_j}, \tag{7}$$

where b_j is the modelled NO_2 concentration at altitude j and the SZA of the SCIAMACHY measurement and a_{kj} the modelled NO_2 concentration at altitude j and SZA k. When tracing the light through the atmosphere from the sun to the balloon borne detector, each point on the line-of-sight can be identified through its altitude and its local SZA. Assuming a layered atmosphere the slant path through layer j at local SZA k is multiplied by κ_{kj}. Hence, we obtain a photochemically corrected weighting function matrix $\tilde{\mathbf{K}}$. Replacing $\mathbf{K}$ by $\tilde{\mathbf{K}}$ in Eq. (1) and solving the inversion problem as described in Sect. 2.1.3 yields the balloon borne trace gas profile scaled to the photochemical conditions of the satellite measurement.

Following a similar approach as in Bracher et al. (2005) the modelling error is estimated by sensitivity studies. For the flight from Kiruna on 24 March 2004, several model runs are performed along a representative air mass trajectory varying model parameters important for the photochemical

variation of NO_2. These parameters include the O_3 profile (-33%, $+50\%$), overhead ozone ($\pm 74\%$), the temperature for each Θ-level (± 7 K), the rate constants of Reactions (R1) and (R2) ($\pm 20\%$), the aerosol surface area ($\pm 40\%$) and the γ-coefficient for N_2O_5 uptake on liquid aerosol (-50%,$+100\%$). For each run two photochemically scaled trace gas profiles are generated corresponding to a backward and a forward satellite match in the morning before and after the balloon flight, respectively. The root mean square deviation of the vertical profiles from the standard run yields the estimate of the modelling error. The modelling error increases from less than 10% at balloon float altitude to 20% at 20 km altitude. Between 20 km and balloon float altitude the error is governed by the factors which influence the photolysis of NO_2 via Eq. (R2). The modelling error for the backward match grows to 30% at 15 km and up to 50% below 15 km, mainly due to the sensitivity of NO_x chemistry to the O_3 profile through Eq. (R1). The modelling error of the forward match calculations remains constant at 20% down to 15 km. Below 15 km it rises up to 35% caused by sensitivity to the O_3 profile. Whenever photochemically corrected trace gas profiles are shown the modelling error is added applying Gaussian error propagation.

Table 1. Compendium of joint LPMA and DOAS balloon flights chosen for comparison. BA, BD, SS and SR indicate balloon ascent, balloon descent, sunset and sunrise, respectively.

Balloon flight date, time/UT	Location	Geophysical condition	Observation geometry
23 Nov. 1996	Leon	mid-lat. fall	
14:56–16:54	42.6° N, 5.7° W	SZA: 74.0°–92.7°	BA, SS
14 Feb. 1997	Kiruna	high-lat. winter	
12.29–14:53	67.9° N, 21.1° E	SZA: 82.7°–94.4°	BA, SS
10 Feb. 1999	Kiruna	high-lat. winter	
11:40–14:52	67.9° N, 21.1° E	SZA: 82.8°–94.6°	BA, SS
25 June 1999	Gap	mid-lat. summer	
04:32–07:46	44.2° N, 4.6° E	SZA: 86.7°–54.7°	BD
21/22 Aug. 2001	Kiruna	high-lat. summer	
16:04–20:05	67.9° N, 21.1° E	SZA: 75.6°–95.8°	BA, SS
01:15–02:30		SZA: 95.4°–90.0°	SR
23 Mar. 2003	Kiruna	high-lat. spring	
14:47–17:28	67.9° N, 21.1° E	SZA: 77.9°–94.7°	BA, SS

3 Internal LPMA/DOAS comparison

3.1 Comparison of LPMA/DOAS O_3 and NO_2 Slant Column Densities

Table 1 summarizes the geophysical conditions of the balloon flights chosen for the comparison of the LPMA/DOAS O_3 and NO_2 SCDs. We present data of six joint LPMA/DOAS balloon flights where the corresponding geophysical conditions range from high-latitude winter and summer to mid-latitude fall comprising measurements inside as well as outside the northern polar vortex. Due to bad data quality or instrumental malfunction and the considerable effort necessary for data re-analysis we restrict the comparison study to six out of the 13 flights conducted to date.

The quality of the LPMA/DOAS comparison is illustrated in Fig. 2 showing O_3 and NO_2 SCDs as well as the corresponding errors and relative deviations inferred from observations at Kiruna on 23 March 2003. The particular flight is chosen as an example since all data sets are available allowing for a consistent comparison. In addition, relative deviations between LPMA and DOAS SCDs are presented as histograms in Figs. 3 and 4 for the six considered balloon flights. Relative deviations are calculated by linear interpolation of the DOAS data to the measurement instances of LPMA.

The general agreement of LPMA and DOAS O_3 SCDs is on the order of 10%. Maximum deviations of up to 30% are observed when slant columns are very low and governed by the O_3 abundances above balloon float altitude indicating a problem when applying Langley's method to retrieve the residual absorber amount in the DOAS solar reference spectrum. For some of the earlier balloon flights the relative deviations for solar occultation measurements are as large as 20%. During solar occultation the measured O_3 IR-absorption lines in the LPMA standard retrieval window become saturated. In order to increase retrieval sensitivity we include a micro-window exhibiting weak, unsaturated O_3 absorption. Unfortunately the latter micro-window is not available for some of the flights due to usage of spectral filters which cut the respective spectral region. The statistical analysis of all 1032 data points yields that in average DOAS O_3 SCDs are larger by 6.1% than the LPMA data. The standard deviation of the relative deviation between LPMA and DOAS amounts to 8.0%, see Fig. 3.

The comparison of NO_2 SCDs is more difficult to assess. The NO_2 measurements during balloon ascent of the earlier flights from Leon in 1996 and Kiruna in 1997 are hard to compare as LPMA data are very noisy. Data retrieved from balloon ascent of the more recent flights at Kiruna in 2001 and in 2003 are less noisy although the NO_2 slant column abundances show similar values. This suggests that the preflight optical alignment of the FT-IR improved during the series of presented balloon flights. For the flights at Kiruna and at Gap in 1999, NO_2 slant columns are close to the detection limit of the LPMA retrieval causing large error bars. The agreement on NO_2 SCDs inferred form solar occultation is on the order of 20%. The maximum deviation up to 50%

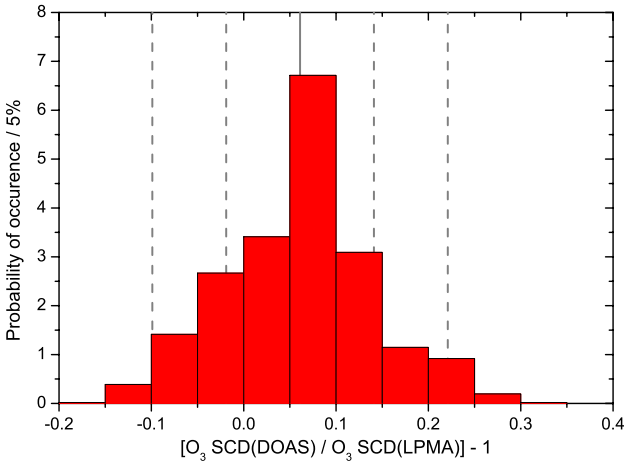

Fig. 3. Histogram of the relative deviations between O_3 SCDs retrieved by DOAS and LPMA, i.e. SCD(DOAS) / SCD(LPMA) - 1. The 1032 data points corresponding to the 6 flights of Table 1 are grouped and counted for occurrence in bins of 5% relative deviation. The mean and the corresponding standard deviation are 6.1% and 8.0%, respectively. The mean value is shown as grey solid line, grey dashed lines correspond to one and two times standard deviation from the mean.

occurs for the flight from Kiruna in 1999 where NO_2 abundances are very low. In this case, stratospheric temperatures were well below 217 K and an extrapolation of the Harder et al. (1997) data has to be used when accounting for the temperature dependence of the NO_2 absorption cross sections. However, an extrapolation error alone cannot account for the observed discrepancy which has been tested using the NO_2 cross section from Bogumil et al. (2003) at 203 K. The statistical analysis of all 1016 data points reveals a mean deviation of +3.7% between DOAS and LPMA with a large standard deviation of 24.5%, see Fig. 4 lower panel. As some of the LPMA data are noisy or close to the detection limit we performed another statistical analysis excluding all data where the corresponding SCDs show errors larger than 25%. The resulting set of 753 data points exhibits a mean relative deviation between DOAS and LPMA of +6.6% and 14.0% standard deviation, see Fig. 4 upper panel. Overall the combined error bars are a reasonable estimate for the LPMA/DOAS agreement on NO_2 measurements.

3.2 Comparison of LPMA/DOAS O_3 and NO_2 profiles

Section 3.1 discussed the level of agreement between the O_3 and NO_2 SCDs inferred from LPMA and DOAS measurements. In this section O_3 and NO_2 data again taken from balloon ascent and sunset of the flight at Kiruna on March 23, 2003, are chosen to illustrate the characteristics of the profile inversion technique. SCDs are inverted to vertical trace gas profiles via Eq. (2). The profile retrieval is characterized by the corresponding averaging kernel matrices given

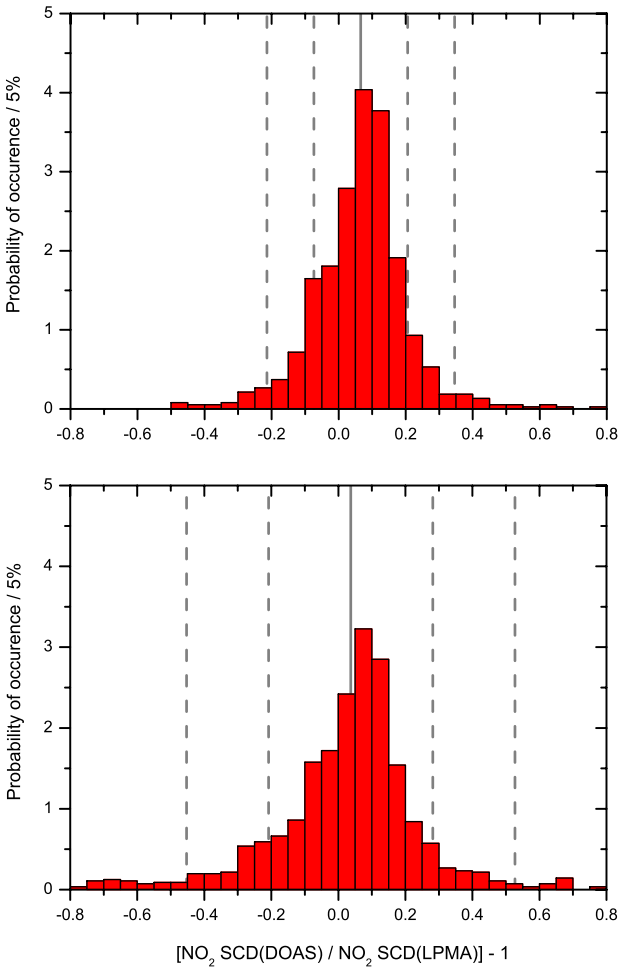

Fig. 4. Histogram of the relative deviations between NO_2 SCDs retrieved by DOAS and LPMA, i.e. SCD(DOAS) / SCD(LPMA) - 1. Lower panel: All 1016 data points corresponding to the 6 flights of Table 1 are grouped and counted for occurrence in bins of 5% relative deviation. The mean and the corresponding standard deviation are 3.7% and 24.5%, respectively. Upper panel: All data where the corresponding SCDs exhibit relative errors larger than 25% are removed. The remaining 753 data are grouped and counted for occurrence in bins of 5% relative deviation. The mean and the corresponding standard deviation are 6.6% and 14.0%, respectively. Common: The mean value is shown as grey solid line, grey dashed lines correspond to one and two times standard deviation from the mean.

by Eq. (5). The O_3 and NO_2 profiles presented in the upper panels of Figs. 5.1 and 5.2, respectively, are retrieved using diagonal a priori covariance matrices with variances corresponding to 30% error of the a priori profiles. LPMA data are inverted on a 2-km altitude grid. DOAS data are generated on the same altitude grid as the satellite retrievals which corresponds to 1 km grid spacing between 10 and 45 km altitude and coarser below and above. In addition DOAS profiles are shown which are smoothed applying Eq. (6) to match

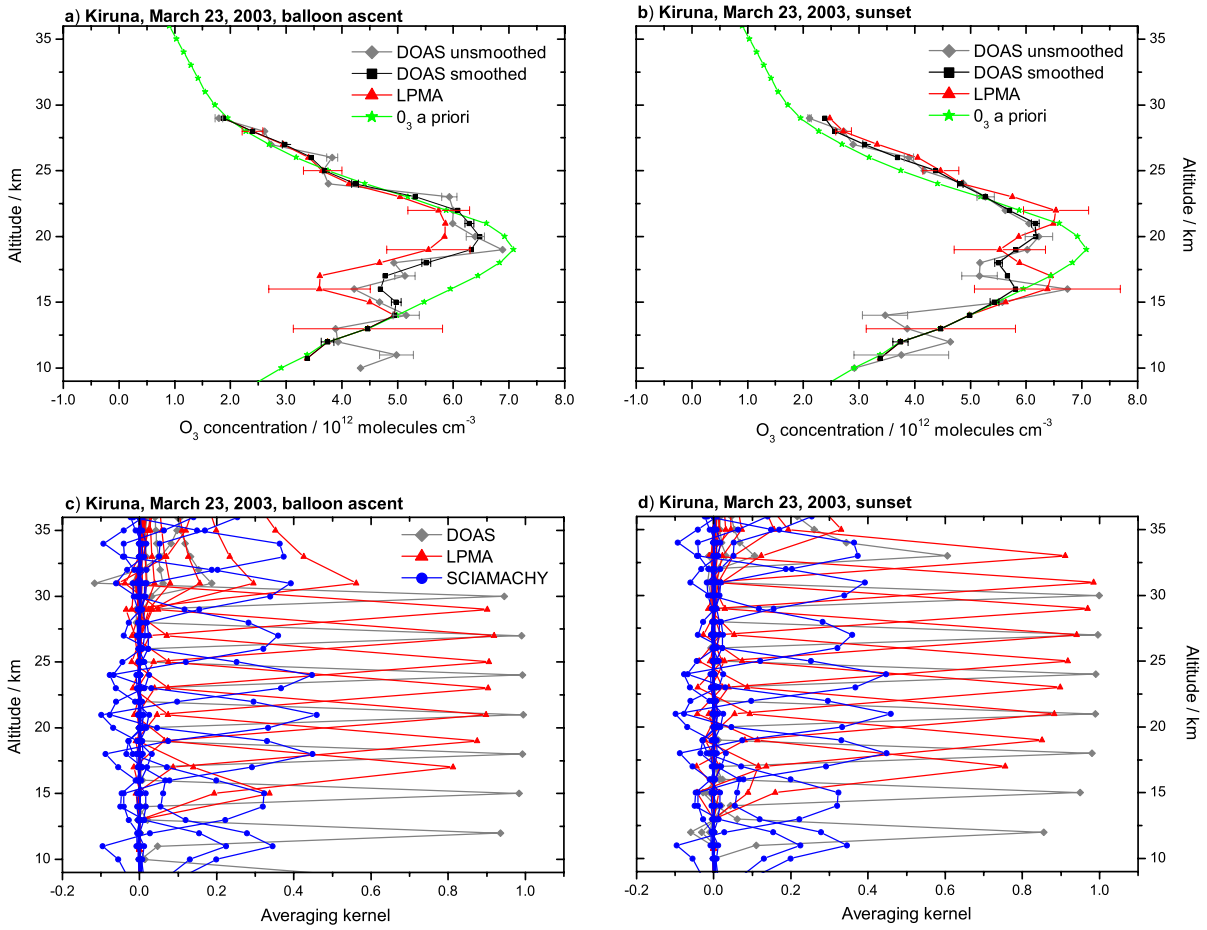

Fig. 5.1. Vertical O_3 profiles (panel **a** and **b**) and corresponding averaging kernels (panel **c** and **d**) retrieved from balloon ascent (panel a and c) and sunset (panel b and d) for the flight from Kiruna on 23 March 2003. LPMA data (red triangles) are retrieved on a 2 km, DOAS data (grey diamonds) on a 1 km altitude grid. In addition smoothed DOAS data are shown (black boxes). The green stars represent the O_3 a priori profile. The averaging kernels of the SCIAMACHY O_3 retrieval are plotted (blue circles) for comparison.

the coarser altitude resolution of LPMA. The corresponding averaging kernels are shown in the lower panels of Fig. 5.1 and 5.2. For comparison, the averaging kernels of the SCIAMACHY limb retrievals (IUP-Bremen) are also plotted.

The retrieved O_3 profiles, Figs. 5.1 and 5.2, reproduce the general behavior of the underlying SCDs shown in Fig. 2. LPMA data underestimate the DOAS data during balloon ascent below 22 km. Above, the agreement is good. During sunset O_3 concentrations retrieved from LPMA spectra tend to be higher than those retrieved from DOAS spectra and the shapes of the considered profiles are somewhat different. The general agreement is on the order of the combined error bars as already indicated by the underlying SCDs.

The averaging kernels of the DOAS O_3 profile retrieval, Fig. 5.1c and d, are well shaped in the altitude range between 10 km and 30 km for both, the balloon ascent and sunset measurements. Hence, profile retrieval is possible with 1 km to 2 km altitude resolution in the respective altitude range. The LPMA averaging kernels are reasonably well shaped between 17 km and balloon float altitude for both viewing geometries and allow for profile retrieval there. Below 17 km, there is essentially no information on the O_3 profile from LPMA measurements, which draws the retrieved profile toward the a priori. Consequently, also the smoothed DOAS profile is drawn toward the LPMA and a priori profile. Filamented structures in the lower stratosphere, e.g. Fig. 5.1b around 15 km, cannot be resolved by the LPMA and smoohed DOAS measurements while they are well resolved by the standard DOAS retrieval. The corresponding altitude resolution of the LPMA balloon ascent and solar occultation measurements improves from about 3 km at 17 km to about 2 km at balloon float altitude. The decrease in altitude resolution for lower altitudes is mostly due to the smaller number of contributing measurements during the beginning of balloon ascent and the increase in vertical averaging by the effective field-of-view of the instruments when the line-of-sight penetrates deeper into the atmosphere during sunset.

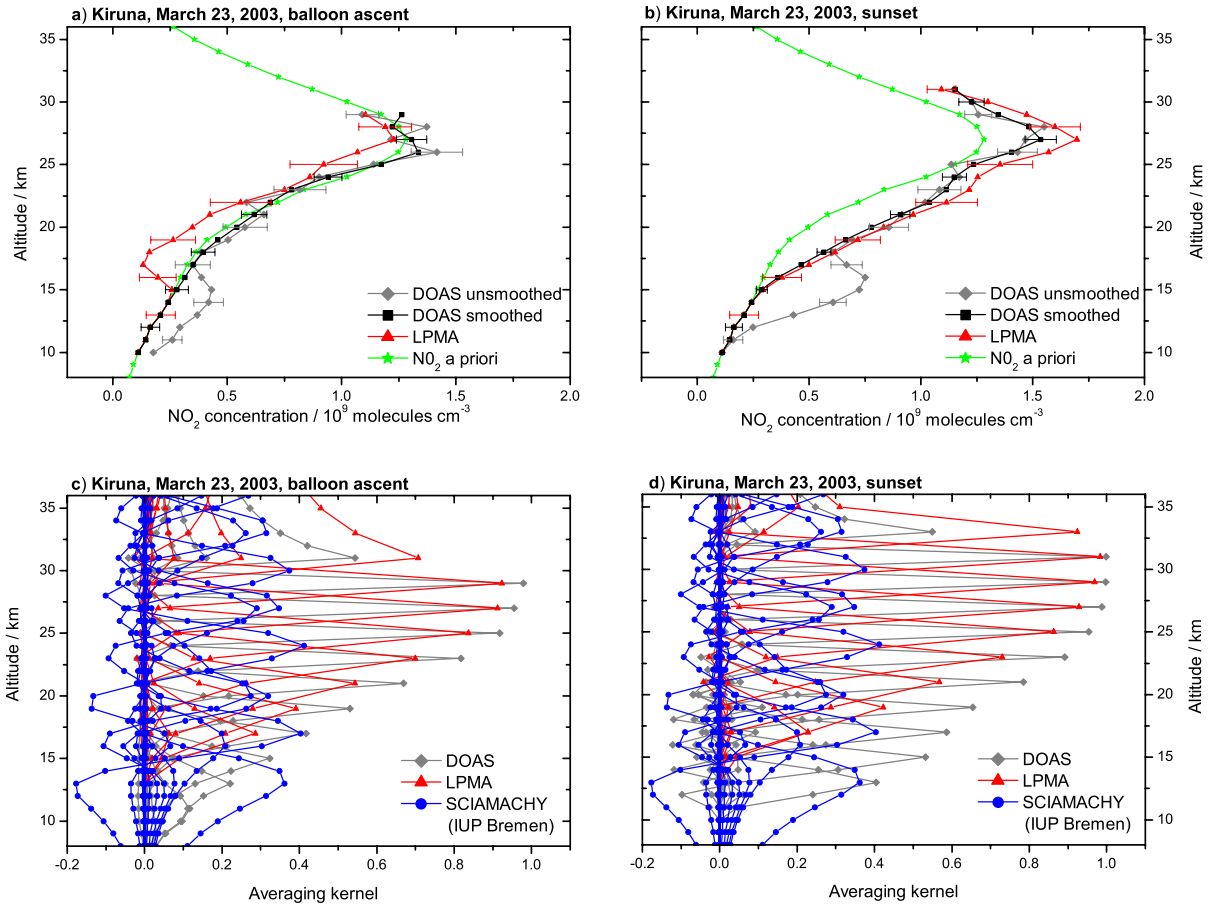

Fig. 5.2. Vertical NO_2 profiles (panel **a** and **b**) and corresponding averaging kernels (panel **c** and **d**) retrieved from balloon ascent (panel a and c) and sunset (panel b and d) for the flight from Kiruna on 23 March 2003. LPMA data (red triangles) are retrieved on a 2 km, DOAS data (grey diamonds) on a 1 km altitude grid. In addition smoothed DOAS data are shown (black boxes). The green stars represent the O_3 a priori profile. The averaging kernels of the SCIAMACHY NO_2 retrieval are plotted (blue circles) for comparison.

The comparison of NO_2 vertical profiles for balloon ascent, Fig. 5.2a, reveals an underestimation of the DOAS by the LPMA data over the entire retrieved altitude range. In the lower stratosphere the discrepancy is substantial and larger than the error bars. For sunset, Fig. 5.2b, LPMA overestimates the DOAS data between 31 km and 25 km. Below 25 km LPMA and DOAS agree well.

The averaging kernels indicate that it is possible to retrieve NO_2 vertical profiles in the range between 12 km and balloon float altitude at about 30 km from DOAS measurements during balloon ascent and sunset exhibiting 5 km to 1 km altitude resolution. However, the NO_2 averaging kernels are less well shaped than those of the O_3 retrieval since the underlying NO_2 SCDs have larger errors. Hence, in contrast to the O_3 retrieval, there is a significant decrease in altitude resolution below 20 km. LPMA measurements during balloon ascent and solar occultation allow for profile retrieval between 17 km and 30 km altitude with 5 km to 2 km altitude resolution. Due to the larger errors of the NO_2 SCDs, altitude resolution for the NO_2 profile retrieval is worse than for the O_3 retrieval. Comparing the averaging kernels of the LPMA and DOAS data sets it becomes evident that smoothing is most significant below 20 km altitude where LPMA measurements yield only little or no information on the NO_2 vertical profile. The secondary (and real) maximum at about 15 km altitude seen in the DOAS unsmoothed data is not present in the LPMA retrieval. Hence, according to Eq. (6) the smoothed DOAS profile is drawn toward the a priori.

For both gases, SCIAMACHY averaging kernels are smaller than 0.5 and significantly broader than the grid spacing indicating that on the selected retrieval grid the retrieved profile points are not independent. Correspondingly, SCIAMACHY's altitude resolution amounts to 3 km to 5 km in the retrieved altitude range.

Table 2. Compendium of joint LPMA and DOAS O_3 and NO_2 profile measurements and Envisat/SCIAMACHY overpasses. BA and SO indicate balloon ascent and solar occultation measurements, respectively.

Balloon flight date, time/UT	Location	Geophysical condition	Available datasets	Satellite coincidence orbit, date, time/UT	Altitude range/km	Time delay/h	Spatial distance/km
04 Mar. 2003	Kiruna	high lat. spring	SO: LPMA	5273, 4 Mar., 11:05	20–30	−5.1	369–496
13:20–16:17	67.9° N, 21.1° E	SZA: 71.1°–94.1°		5285, 5 Mar., 7:17	23–24	+15.3	498–499
23 Mar. 2003	Kiruna	high lat. spring	BA: LPMA, DOAS	5545, 23 Mar., 11:07	18–28	−5.2	268–496
14.47–17:28	67.9° N, 21.1° E	SZA: 78.9°–94.7°		5558, 24 Mar., 9:01	19–29	+17.4	10–495
			SO: LPMA, DOAS	5545, 23 Mar., 11:07	20–30	−6.2	63–458
				5558, 24 Mar., 9:01	17–30	+16.0	256–453
9 Oct. 2003	Aire sur l'Adour	mid-lat. fall	BA: DOAS	8407, 9 Oct., 9:51	17–31	−6.5	738–988
15:39–17:09	43.7° N, 0.3° W	SZA: 72.0°–87.8°		8421, 10 Oct., 9:20	25–33	+17.2	547–977
24 Mar. 2004	Kiruna	high lat. spring	BA: DOAS	10798, 24 Mar., 10:35	12–33	−5.4	371–499
14:04–17:31	67.9° N, 21.1° E	SZA: 74.5°–95.3°		10812, 25 Mar., 10:04	6–16	+19.9	32–485
			SO: DOAS	10798, 24 Mar., 10:35	10–33	−6.9	191–436
				10812, 25 Mar., 10:04	10–20	+16.7	301–475
17 June 2005	Teresina	tropical winter	BA: in preparation	17240, 17 June, 11:53	25–30	−8.1	382–491
18:32–21:13	5.1° S, 42.9° W	SZA: 60.6°–95.8°		17255, 18 June, 13:02	5–33	+18.4	6–490
			SO: in preparation	17240, 17 June, 11:53	23–32	−9.1	519–971
				17255, 18 June, 13:02	8–33	+16.2	12–496

3.3 Conclusions on the LPMA/DOAS comparison and implications for satellite validation

As presented in Sects. 3.1 and 3.2, O_3 and NO_2 abundances inferred from LPMA/DOAS measurements in the IR and visible spectral ranges agree roughly within $\pm 10\%$ for O_3 and $\pm 20\%$ for NO_2. Observed discrepancies can be due to instrumental and retrieval related shortcomings of either technique. The LPMA Fourier Transform spectrometer inherently exhibits smaller signal-to-noise-ratio (SNR$\simeq 10^2$) than the grating spectrometers operated by DOAS (SNR$\simeq 10^4$) causing significantly smaller detection limit and higher precision of the DOAS measurements. In the visible spectral range where the Sun's intensity peaks the typical integration time for individual spectra is less than 1 s, whereas in the IR it takes about 50 s to record a single interferogram. Hence, the DOAS instruments sample the atmosphere with a much higher rate than the LPMA FT-IR. Taking into account the respective errors of the considered trace gases it is evident that altitude resolution is significantly better for the DOAS observations. When the apparent size of the solar disk becomes large during solar occultation the smaller field of view of the FT-IR (FOV$\simeq 0.2°$) partly compensates the high integration times and large errors compared to the DOAS measurements (FOV$\simeq 0.53°$). On the other hand the small field of view of the FT-IR renders the intensity of the measured interferograms very sensitive to small pointing errors of the sun-tracker as the solar irradiance is not uniform across the solar disk (Bösch et al., 2003). According to Fig. 3 and 4 LPMA O_3 and NO_2 SCDs are low biased with respect to the corresponding DOAS SCDs. For both trace gases the typical errors of individual measurements are larger than the bias. Errors of the absorption cross sections with respect to magnitude or pressure and temperature dependencies would directly cause a bias. Especially the DOAS retrieval of NO_2 might exhibit shortcomings when accounting for the temperature dependence of the NO_2 absorption cross section, since the interpolation is performed linearly using four reference temperatures, only. In the IR spectral range, errors in the spectroscopic parameters and the ambient temperature and pressure data propagate into the shape of the absorption lines causing systematic errors of the retrieved trace gas SCDs. Correlations between the various fitting parameters considered for the spectral retrieval are minimized but, still, might cause small unaccounted systematic errors in both data sets. Summing up the arguments, the O_3 and NO_2 stratospheric profiles inferred from DOAS measurements appear to be better suited for validation purposes than the LPMA data particularly as the former exhibit smaller error bars and better altitude resolution. Nonetheless, stratospheric FT-IR measurements are indispensable since the majority of trace gases important for a comprehensive understanding of stratospheric photochemistry do not absorb in the UV/visible.

4 Validation of SCIAMACHY O_3 and NO_2 profiles

4.1 Observations

The validation study reports on four LPMA/DOAS balloon flights, three from ESRANGE, Kiruna, Sweden, and one from Aire sur l'Adour in southern France conducted since 2003. The analysis of a fifth balloon flight at Teresina, Brazil, in June 2005 is currently in preparation. For each balloon flight a satellite coincident measurement is identified in the morning before and after the balloon flight using the trajectory matching technique described in Sect. 2.3. In the following we refer to these coincidences as backward and forward coincidences. If trace gas profiles inferred from balloon ascent and solar occultation are available the satellite coincidences are identified separately. For each balloon flight Table 2 provides information on the measurement site, the geophysical condition, the SZA range covered by the balloon borne observations, the available data sets and some details on the selected SCIAMACHY limb scans. Besides orbit number, time and date of the satellite measurement, the matching altitude range, the distance with respect to the air masses probed by the balloon borne instruments and the time delay between satellite overpass and balloon flight are given.

In general we succeed in identifying satellite coincidences in the altitude range from about 20 km to 30 km. In some cases the characteristics of the satellite coincidences are not perfect for validation purposes, e.g. for the flight from Kiruna in 2004 where the coincident altitude range is below 20 km and for the flight from Kiruna on 4 March 2003, where the forward coincidence is restricted to a small altitude range. Nevertheless, remembering that coincidence criteria are somewhat arbitrary the balloon and satellite borne trace gas profiles are compared in the whole retrieved altitude range. For the flight from Aire sur l'Adour on 9 October 2003, the match criterion is weakened to a maximum spatial mismatch of 1000 km, as no coincidence is found applying the 500 km criterion. Furthermore assuming the weakened match criterion, the satellite overpass in the morning of 9 October coincides directly with the balloon measurement locations. Hence, the backward model calculations for this flight are not performed along the SZA timeline given by air mass trajectory calculations, but are carried out along the SZA timeline corresponding to air masses stationary at Aire sur l'Adour.

The retrieved vertical trace gas profiles for O_3 and NO_2 are shown in Figs. 6 and 7, respectively. Satellite observations in the morning before and after the balloon flight are compared to balloon borne trace gas profiles. We present smoothed and in the case of NO_2 also photochemically corrected balloon borne profiles. For reference vertical profiles without photochemical correction at full altitude resolution are plotted. In the case of O_3, in-situ sonde data are included if available. The O_3 sonde data are taken from an electrochemical cell either deployed onboard the gondola or launched from the ground station shortly after balloon launch. The relative deviations between the satellite and balloon borne measurements are assessed in Figs. 8 and 9 for O_3 and NO_2, respectively.

LPMA data are available for the two flights at Kiruna in 2003, only. DOAS data are lacking for 4 March 2003, due to instrumental malfunction. According to the findings of Sect. 3.2, DOAS O_3 and NO_2 profiles are retrieved on the same altitude grid as the satellite profiles. As the altitude resolution of the DOAS retrieval is significantly better, DOAS profiles are smoothed to match the satellite's coarser altitude resolution except for NO_2 at balloon ascent below 20 km where no smoothing is applied. LPMA trace gas profiles are generated on a 2-km altitude grid applying no smoothing as the satellite's altitude resolution does not differ significantly. Satellite borne O_3 profiles are inferred using the IUP-Bremen retrieval algorithm. SCIAMACHY NO_2 profiles are generated by the IUP-Bremen and Harvard retrieval. In two cases also NO_2 profiles inferred by the IUP-Heidelberg are available. Relative deviations between balloon and satellite borne observations are calculated for the trace gas profiles retrieved at the IUP-Bremen and the balloon borne DOAS measurements, except for the observations at Kiruna on 4 March 2003, where LPMA data are used in the absence of available DOAS measurements.

4.2 Discussion

4.2.1 O_3 validation study

The internal consistency of the validation data set has been discussed in Sect. 3.1 where a bias of +6.1% between DOAS and LPMA O_3 measurements is detected. The corresponding standard deviation of the deviations between the two datasets is 8.0%. Accordingly, the inferred vertical profiles mostly agree to within the combined error bars of both data sets. In all cases the agreement between in-situ sonde and remote sensing balloon borne O_3 data is good. Sometimes even highly filamented structures, e.g. Fig. 6e, can be observed simultaneously in the high resolution balloon borne and the in-situ observations.

Figures 6 and 8 show the O_3 satellite validation study. In most cases SCIAMACHY limb O_3 profiles agree to within $\pm 20\%$ with the validation data set in the 20 km to 30 km altitude range. The agreement ranges from close to perfect as for the observations at Kiruna on 4 March 2003, Fig. 6a, to fair as in the case of Fig. 6d, Aire sur l'Adour on 9 October 2003, where the agreement in the considered altitude range is on the order of 30%, only, and the profile shape is rather different for satellite and balloon borne data. The relative deviations show a systematic underestimation of the balloon borne by the satellite borne profiles at 24 km to 28 km altitude. The underestimation decreases and sometimes changes to overestimation when going up to 31 km and down to 20 km. This finding is similar to conclusions of Brinksma et al. (2005),

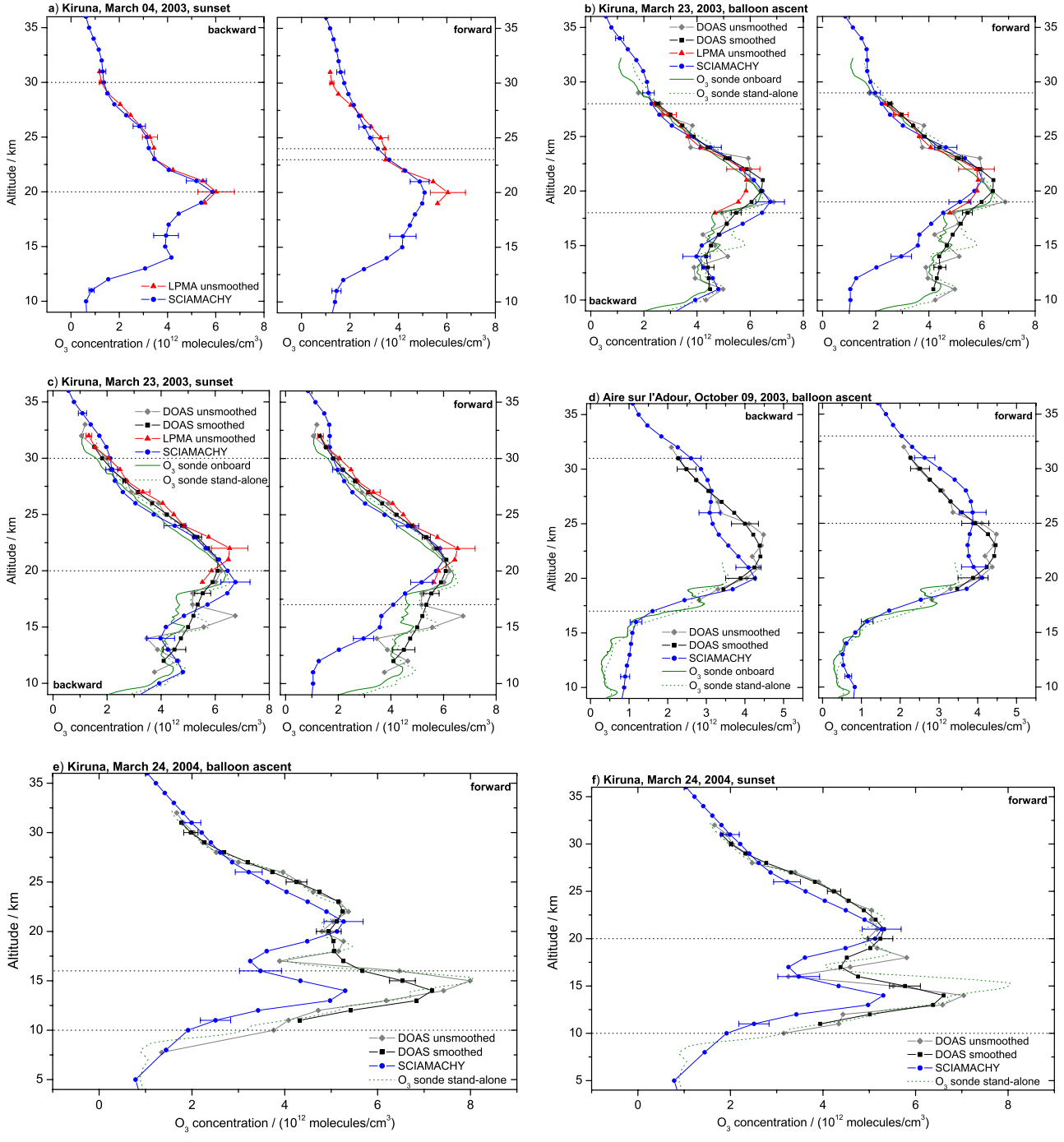

Fig. 6. Comparison of O_3 profiles inferred from SCIAMACHY limb observations with correlative balloon borne measurements. Panels (a) to (f) correspond to observations at **(a)** Kiruna on 4 March 2003, at Kiruna on 23 March 2003, during **(b)** balloon ascent and **(c)** sunset, at **(d)** Aire sur l'Adour on 9 October 2003 and at Kiruna on 24 March 2004, during **(e)** balloon ascent and **(f)** sunset. The left and right sub-panels correspond to backward and forward coincidences. Satellite data are shown as blue circles. Smoothed DOAS data are plotted as black boxes, LPMA data as red triangles. The grey diamonds represent DOAS O_3 profiles at full altitude resolution without smoothing. If available, O_3 profiles measured by an electrochemical cell onboard the gondola during balloon ascent are shown as green line. The dashed green lines correspond to O_3 profiles inferred from stand-alone in-situ sondes launched from the ground station shortly after balloon launch. The altitude range between the horizontal dotted lines represents the range where coincident air masses are found. Unfortunately on 24 March 2004, only forward match data are available for SCIAMACHY. For better visibility, only selected error bars are shown.

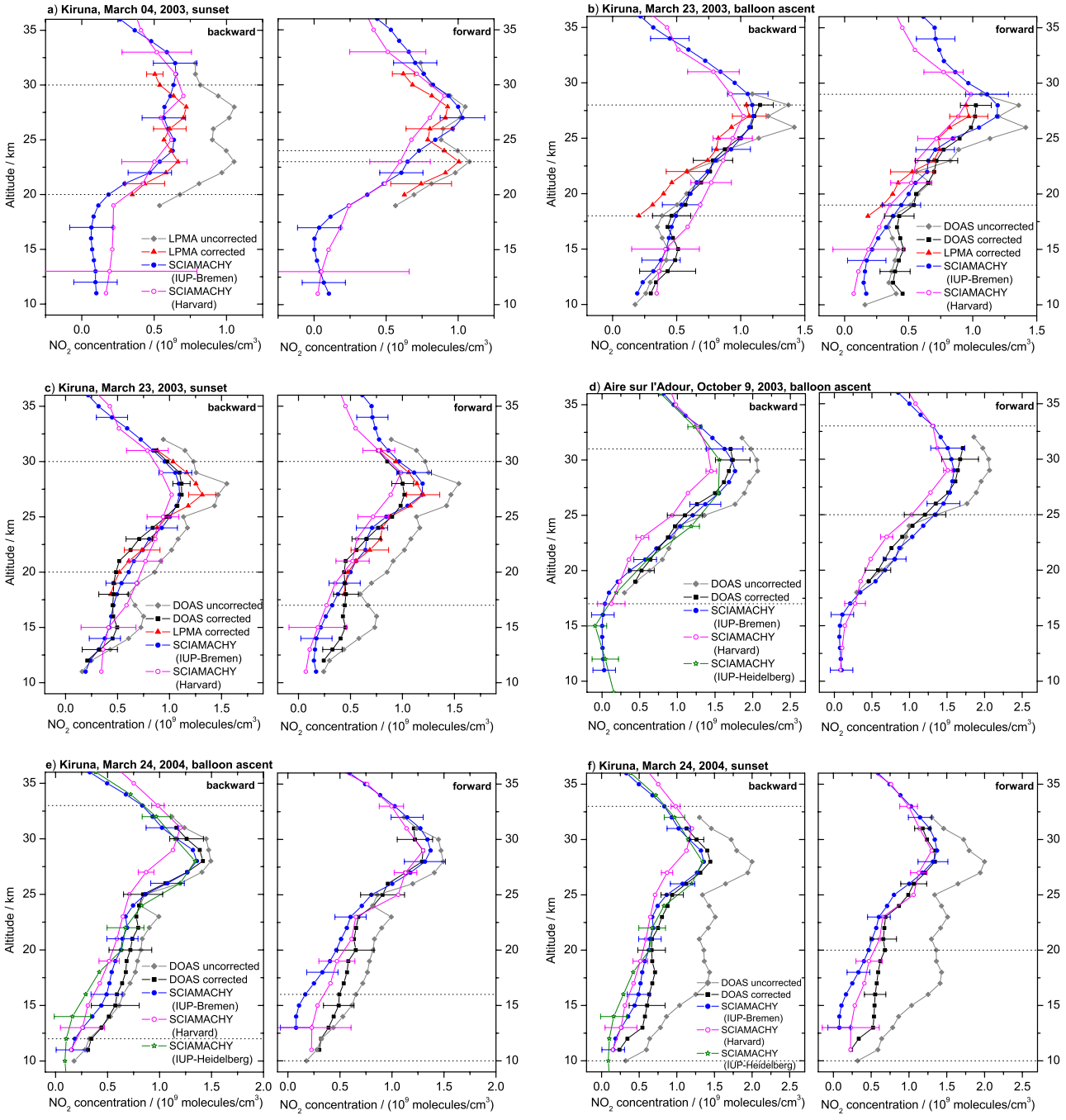

Fig. 7. Comparison of NO_2 profiles inferred from SCIAMACHY limb observations with correlative balloon borne measurements. Panels **(a)** to **(f)** correspond to observations at (a) Kiruna on 4 March 2003, at Kiruna on 23 March 2003, during (b) balloon ascent and (c) sunset, at (d) Aire sur l'Adour on 9 October 2003 and at Kiruna on 24 March 2004, during (e) balloon ascent and (f) sunset. The left and right sub-panels correspond to backward and forward coincidences. Satellite data inferred by IUP-Bremen are shown as blue full circles, inferred by Harvard as open magenta circles, inferred by IUP-Heidelberg as green open stars. Photochemically corrected and smoothed DOAS data are plotted as black boxes, photochemically corrected LPMA data as red triangles. The grey diamonds represent balloon borne profiles at full altitude resolution without photochemical correction which are taken from the DOAS data except for the flight from Kiruna on 4 March 2003, where LPMA data are used. The altitude range between the horizontal, dotted lines represents the range where coincident air masses are found. For better visibility, only selected error bars are shown.

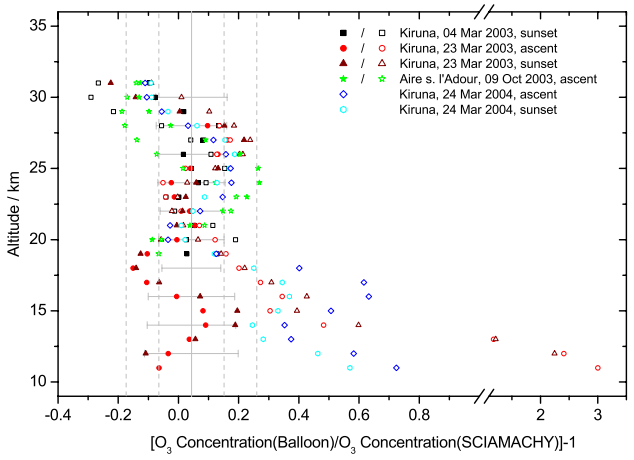

Fig. 8. Relative deviations between satellite and balloon borne measurements of O_3 profiles. Filled and open symbols correspond to backward and forward coincidences, respectively. Observation sites and conditions are indicated in the legend. The mean deviation of all coincident data in the 20 km–31 km altitude range is 4.3% with 10.8% standard deviation. The grey lines indicate the mean at +0.043 and the one and two times standard deviation boundaries with respect to the 20 km–31 km altitude range. The grey error bars indicate the mean combined errors of the satellite and balloon borne observations. Note the broken abscissa.

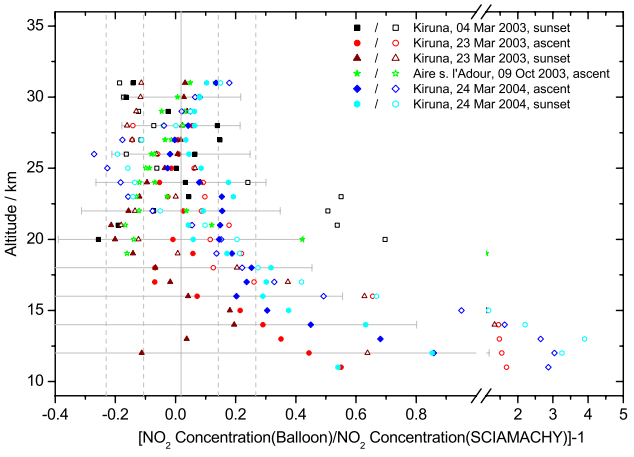

Fig. 9. Relative deviations between satellite (IUP-Bremen) and balloon borne measurements of NO_2 profiles. Filled and open symbols correspond to backward and forward coincidences, respectively. Observation sites and conditions are indicated in the legend. SCIAMACHY data corresponding to the backward coincidence on 4 March 2003, at Kiruna are shifted by −2 km. The mean deviation of all coincident data in the 20 km–31 km altitude is 1.8% with 12.4% standard deviation. The grey lines indicate the mean at 0.018 and the one and two times standard deviation boundaries with respect to the 20 km–31 km altitude range. The grey error bars indicate the mean combined errors of the satellite and balloon borne observations including modelling error. Note the broken abscissa.

where a zigzag shape of the deviations between a validation data set (lidar, SAGE II) and the IUP-Bremen O_3 retrieval is observed, indicating that O_3 concentrations at 27 km inferred from SCIAMACHY limb are too low. Albeit different corrections for tangent height errors are already included in the SCIAMACHY retrievals there might be a remaining small tangent height error causing the observed deviations. The combined error bars of the balloon and satellite borne observations are on the order of the observed standard deviation of all coincident measurements in the 20 to 30 km altitude range. However, a number of data points differ by more than the combined error bars which might point to a systematic error as suggested above.

Below 20 km SCIAMACHY O_3 profiles underestimate the balloon borne data in most cases and cannot reproduce the frequently highly filamented O_3 profiles observed especially at high latitudes during winter, e.g. Fig. 6e and f. The balloon flights from Kiruna on 23 March 2003, and on 24 March 2004, have been conducted close to the polar vortex edge where the gradients in O_3 concentration are large on small spatial scales. When identifying coincident balloon and satellite measurements, the air mass trajectory calculations allow for a sizeable mismatch in space and time. Spatial mismatch of up to 500 km is possible and, hence, the influence of horizontally inhomogeneous air masses can be important close to the polar vortex edge. Further, SCIAMACHY measurements represent an average over a 960 km wide horizontal area, whereas the LPMA/DOAS measurements average the horizontal trace gas distribution along the line-of-sight from the balloon to the sun. Deviations as in Fig. 6e and f might originate from the difference in horizontal averaging. Good agreement is found for the backward coincidences in Fig. 6b and c. However, the forward coincident measurements in Fig. 6b, c, e and f show large deviations between satellite and balloon borne data. Since the uncertainty of the air mass trajectory calculations increases with increasing time-lag to initialization of the trajectory model, the influence of horizontally inhomogeneous air masses might be enhanced for the forward calculations where the time-lag is about ten hours larger than in the backward case. Unfortunately, there are no DOAS or LPMA data available for the observations below 19 km at the mid-latitudinal station Aire sur l'Adour, but SCIAMACHY limb profiles and the corresponding profiles inferred from in-situ O_3 sondes agree well, see Fig. 6d. Figure 8 reveals that the combined error bars cannot explain the observed discrepancies below 20 km altitude.

4.2.2 NO_2 validation study

The internal agreement of the balloon borne NO_2 measurements has been assessed in Sects. 3.1 and 3.2. When neglecting noisy data, we observe a bias of +6.6% of the DOAS with respect to the LPMA observations, the standard deviation of the relative differences is 14.0%. Accordingly, the

LPMA/DOAS observations in Fig. 7b and c mostly lie within the combined error bars. Nonetheless, for the flight from Kiruna on 23 March 2003, LPMA underestimates the DOAS profile for balloon ascent and overestimates it for sunset as already seen in Fig. 5.2. Remarkable agreement can be observed for DOAS profiles retrieved from measurements during balloon ascent and sunset which are scaled to the photochemical regime of the same SCIAMACHY observation, proofing the validity of our photochemical as well as meteorological approach.

The comparison between NO_2 profiles inferred from the SCIAMACHY limb measurements and the validation data set is presented in Figs. 7 and 9. Although a detailed comparison of the different retrieval exercises is beyond the scope of the present study, we note that the internal agreement of the satellite data is variable. NO_2 profiles inferred by IUP-Bremen and IUP-Heidelberg show good agreement. Deviations are observed for 9 October 2003, Fig. 7d, at 30 km altitude and for 24 March 2004, Fig. 7e, below 20 km. In some cases, e.g. Fig. 7d, the Harvard NO_2 retrieval yields smaller trace gas concentrations than the IUP-Bremen algorithm around 25 to 27 km altitude. In one case, the backward coincidence in Fig. 7e and f, where SCIAMACHY was operating in a non-nominal measurement mode and pointing could not be verified, the Harvard profiles are offset by +2 km to +3 km with respect to the other satellite data. For the forward coincidence at Kiruna in 2004, agreement is good. In the following we refer our discussion to the IUP-Bremen records as the latter agree best with the balloon borne data. Implications for the Harvard and IUP-Heidelberg retrievals can be inferred easily.

In the 20 km to 30 km altitude range the agreement between the balloon borne NO_2 profiles and the satellite observations is on the order of 20% and most often well represented by the combined error bars. The latter amount to about 1.5 to 3 times the observed standard deviation between the two data sets for all coincident datapoints in the considered altitude range. No clear trend can be observed except for the backward observations at Kiruna on 4 March 2003, Fig. 7a, where an altitude offset of +2 km to +3 km of the SCIAMACHY with respect to the LPMA data is clearly visible. The same might be true for the forward coincidences at Kiruna in 2004, Fig. 7e and f, but the offset is not as clear as for the former comparison.

Below 20 km the level of agreement is variable. Similar to the O_3 comparison, the backward coincidences in Fig. 7b, c, e and f reveal moderate deviations whereas the corresponding forward coincidences exhibit larger differences between the satellite and the balloon borne measurements. Further, as can been seen in Fig. 7e, the SCIAMACHY limb profiles retrieved by the IUP-Bremen, IUP-Heidelberg and Harvard algorithms exhibit sizeable discrepancies below 20 km. This indicates that for low altitudes the SCIAMACHY retrieval might depend on the actual parameters, e.g. a priori information, used. The latter finding is supported by the characteristics of the corresponding averaging kernels, Fig. 5.2, which grow wider below 20 km altitude. The combined relative errors shown in Fig. 9 increase dramatically with decreasing altitude since, there, the absolute abundances of NO_2 are very low. The relative errors of SCIAMACHY NO_2 measurements below 15 km typically are larger than 50%. Adding the rather large modelling error and the error of the balloon borne measurements, the combined error bars are often on the order of the observed deviation. Despite the large combined error bars, a systematic underestimation of the balloon by the satellite borne data is obvious.

5 Conclusions

Stratospheric O_3 and NO_2 abundances inferred from different sensors are inter-compared.

In the first part of this study line-of-sight absorptions and vertical profiles retrieved from the UV/vis DOAS spectrometer and the LPMA FT-IR both performing balloon borne direct sun measurements during balloon ascent and solar occultation are compared. The general agreement is $\pm$10% and $\pm$20% for O_3 and NO_2, respectively. The observations in the visible wavelength range exhibit higher precision and better altitude resolution than the FT-IR measurements due to lower instrumental noise and higher sampling frequency. In solar occultation, the smaller field of view of the FT-IR partly compensates the deficiency in altitude resolution. A small bias between the data inferred from the visible and from the IR observed for both gases could be explained by errors of the spectroscopic parameters, i.e. absorption cross sections and their pressure and temperature dependencies, or remaining correlations between the retrieval parameters. However, the bias lies within the errors of individual measurements.

The second part of this study addresses the validation of O_3 and NO_2 stratospheric profiles inferred from SCIAMACHY skylight limb observations based on the balloon borne data set presented in the first part. An air mass trajectory model is used to identify coincident balloon and satellite borne measurements. The balloon borne trace gas profiles are treated appropriately to match the altitude resolution of the satellite sensor and in the case of NO_2 by means of a 1-D stratospheric chemistry model to match the photochemical conditions of the satellite measurements. Typical deviations between SCIAMACHY observations and balloon borne data amount for both considered gases to 20% in the 20 km to 30 km altitude range, somewhat depending on the retrieval algorithm. In the case of O_3 our observations support findings of a previous study (Brinksma et al., 2005) indicating that the IUP-Bremen O_3 retrievals are systematically low between 24 km and 28 km altitude. Below 20 km the agreement worsens for both gases due to the lower sensitivity of the satellite retrieval, uncompensated horizontal variations of the trace gases and in the case of NO_2, modelling uncertainty. Since the origin of the discrepancies observed at low altitudes

cannot be unambiguously attributed to the satellite retrievals or the validation strategy, it is important for future studies to keep the spatial and temporal mismatch between satellite and validation measurements as small as possible. The internal agreement of the satellite NO_2 retrieval exercises developed by IUP-Bremen, Harvard and IUP-Heidelberg, is promising.

Finally, the present study provides a data set which can contribute to the improvement and the validation of future official ESA algorithms currently under development.

The presented balloon borne profiles are made available to the public via our web-site http://www.iup.uni-heidelberg.de/institut/forschung/groups/atmosphere/stratosphere/.

Acknowledgements. The present work has been conducted within ESA contracts AO 146 and AO 465 and funding came through the Bundesministerium für Bildung und Forschung (BMBF) contracts BMBF-07UFE12/8, DLR-50EE0017, and DLR-50EE0027 and the European Union (project TOPOZ-III, EVK2-CT-2001-00102). Some data shown here were calculated on HLRN (High-Performance Computer Center North). Services and support are gratefully acknowledged. Additional support was provided by Vernetzungsfonds of the German Helmholtz-Gemeinschaft and the European Space Agency through the ESABC project. The ECMWF data are made available by the German Weather Service (Deutscher Wetterdienst, DWD). In particular, we thank the team of CNES for the assistance given to perform successfully the balloon flights, and the offered hospitality and support of the SSC team from Esrange/Sweden and the CNES team from Aire sur l'Adour/France.

Edited by: H. Kelder

References

Anderson, S. and Mauersberger, K.: Laser measurements of ozone absorption cross sections in the Chappuis band, Geophys. Res. Lett., 19(9), 933–936, 1992.

Bacmeister, J. T., Kuell, V., Offermann, D., Riese, M., and Elkins, J. W.: Intercomparison of satellite and aircraft observations of ozone, CFC-11, and NO(y) using trajectory mapping, J. Geophys. Res., 104(D13), 16 379–16 390, 1999.

Bogumil, K., Orphal, J., Voigt, S., Bovensmann, H., Fleischmann, O. C., Hartmann, M., Homann, T., Spietz, P., Vogel, A., and Burrows, J. P.: Reference Spectra of Atmospheric Trace Gases Measured by the SCIAMACHY PFM Satellite Spectrometer, Proc. 1st Europ. Sympos. Atmos. Meas. from Space (ESAMS-99), Vol. 2, ISSN 1022-6656, ESA-ESTEC, Noordwijk, 443–447, 1999.

Bogumil, K., Orphal, J., Homann, T., Voigt, S., Spietz, P., Fleischmann, O. C., Vogel, A., Hartmann, M., Bovensmann, H., Frerik, J., and Burrows, J. P.: Measurements of Molecular Absorption Spectra with the SCIAMACHY Pre-Flight Model: Instrument Characterization and Reference Data for Atmospheric Remote-Sensing in the 230-2380 nm Region, J. Photochem. Photobiol. A., 157, 167–184, 2003.

Bösch, H., Camy-Peyret, C., Chipperfield, M., Fitzenberger, R., Harder, H., Schiller, C., Schneider, M., Trautmann, T., and Pfeilsticker, K.: Intercomparison of measured and modeled stratospheric UV/vis actinic fluxes at large solar zenith angles, Geophys. Res. Lett., 28, 1179–1182, 2001.

Bösch, H., Camy-Peyret, C., Chipperfield, M. P., Fitzenberger, R., Harder, H., Platt, U., and Pfeilsticker, K.: Upper limits of stratospheric IO and OIO inferred from center-to-limb-darkening-corrected balloon-borne solar occultation visible spectra: Implications for total gaseous iodine and stratospheric ozone, J. Geophys. Res., 108(D15), 4455, doi:10.1029/2002JD003078, 2003.

Bracher, A., Sinnhuber, M., Rozanov, A., and Burrows, J. P.: Using a photochemical model for the validation of NO_2 satellite measurements at different solar zenith angles, Atmos. Chem. Phys., 5, 393-408, 2005.

Brinksma, E. J., Bracher, A., Lolkema, D. E., Segers, A. J., Boyd, I. S., Bramstedt, K., Claude, H., Godin-Beekmann, S., Hansen, G., Kopp, G., Leblanc, T., McDermid, I. S., Meijer, Y. J., Nakane, H., Parrish, A., von Savigny, C., Strebel, K., Swart, D. P. J., Taha, G., and Piters, A. J. M.: Geophysical validation of SCIAMACHY Limb Ozone Profiles, Atmos. Chem. Phys., 6, 197–209, 2006.

Burkholder, J. B. and Talukdar, R. K.: Temperature dependence of the ozone absorption cross section over the wavelength range 410 to 760 nm, Geophys. Res. Lett., 21, 581–584, 1994.

Burrows, J. P., Hölzle, E., Goede, A. P. H., Visser, H., and Fricke, W.: SCIAMACHY – Scanning Imaging Absorption Spectrometer for Atmospheric Chartography, Acta Astronautica, 35(7), 445–451, 1995.

Bovensmann, H., Burrows, J. P., Buchwitz, M., Frerick, J., Noël, S., Rozanov, V. V., Chance, K. V., and Goede, A. P. H.: SCIAMACHY: Mission Objectives and Measurement Modes, J. Atmos. Sci., 56, 127–150, 1999.

Camy-Peyret, C., Flaud, J.-M., Perrin, A., Rinsland, C. P., Goldman, A., and Murcray, F.: Stratospheric N_2O_5, CH_4 and N_2O profiles from IR solar occultation spectra, J. Atmos. Chem., 16, 31–40, 1993.

Camy-Peyret, C.: Balloon-borne Fourier transform spectroscopy for measurements of atmospheric trace gases, Spectrochim. Acta, 51A, 1143–1152, 1995.

Chipperfield, M. P.: Multiannual simulations with a 3-D CTM, J. Geophys. Res., 1104, 1781–1806, 1999.

Cohen, R. C., Perkins, K. K., Koch, L. C., Stimpfle, R. M., Wennberg, P. O., Hanisco, T. F., Lanzendorf, E. J., Bonne, G. P., Voss, P. B., Salawitch, R. J., Del Negro, L. A., Wilson, J. C., McElroy, C. T., and Bui, T. B.: Quantitative constraints on the atmospheric chemistry of nitrogen oxides: An analysis along chemical coordinates, J. Geophys. Res., 105, 24 283-24 304, 2000.

Connor, B. J., Siskind, D. E., Tsou, J. J., Parrish, A., and Remsberg, E. E.: Ground-based microwave observations of ozone in the upper stratosphere and mesosphere, J. Geophys. Res., 99(D8), 16 757-16 770, 1994.

Crutzen, P. J.: The influence of nitrogen oxides on the atmospheric ozone content, Q. J. R. Meteorol. Soc., 96, 320–325, 1970.

Danilin, M. Y., Ko, M. K. W., Froidevaux, L., Santee, M. L., Lyjak, L. V., Bevilacqua, R. M., Zawodny, J. M., Sasano, Y., Irie, H., Kondo, Y., Russell, J. M., Scott, C. J., and Read, W. G.: Trajectory hunting as an effective technique to validate multiplatform measurements: Analysis of the MLS, HALOE, SAGE-II, ILAS, and POAM-II data in October–November 1996, J. Geophy. Res., 107(D20), 4420, doi:10.1029/2001JD002012, 2002a.

Danilin, M. Y., Ko, M. K. W., Bevilacqua, R. M., Lyjak, L. V., Froidevaux, L., Santee, M. L., Zawodny, J. M., Hoppel, K. W.,

Richard, E. C., Spackman, J. R., Weinstock, E. M., Herman, R. L., McKinney, K. A., Wennberg, P. O., Eisele, F. L., Stimpfle, R. M., Scott, C. J., Elkins, J. W., and Bui, T. V.: Comparison of ER-2 aircraft and POAM III, MLS, and SAGE II satellite measurements during SOLVE using traditional correlative analysis and trajectory hunting technique, J. Geophys. Res., 107, 8315, doi:10.1029/2001JD000781, 2002b.

Del Negro, L. A., Fahey, D. W., Gao, R. S., Donnelly, S. G., Keim, E. R., Neuman, J. A., Cohen, R. C., Perkins, K. K., Koch, L. C., Salawitch, R. J., Lloyd, S. A., Proffitt, M. H., Margitan, J. J., Stimpfle, R. M., Bonne, G. P., Voss, P. B., Wennberg, P. O., McElroy, C. T., Swartz, W. H., Kusterer, T. L., Anderson, D. E., Lait, L. R., and Bui, T. B.: Comparison of modeled and observed values of NO_2 and $J(NO_2)$ during the Photochemistry of Ozone Loss in the Artic Region in Summer (POLARIS) mission, J. Geophys. Res., 104, 26 687-26 703, 1999.

Deshler, T., Hervig, M. E., Hofmann, D. J., Rosen, J. M., and Liley, J. B.: Thirty years of in situ stratospheric aerosol size distribution measurements from Laramie, Wyoming (41N), using balloonborne instruments, J. Geophys. Res., 108, 4167-4179, 2003.

Dobson, G.M.B.: Observers' handbook for the ozone spectrophotometer, Ann. IGY, 5, 46–89, 1957a.

Dobson, G.M.B.: Adjustment and calibration of the ozone spectrophotometer, Ann. IGY, 5, 90–114, 1957b.

Dufour, G., Payan, S., Lefévre, F., Eremenko, M., Butz, A., Jeseck, P., Té, Y., Pfeilsticker, K., and Camy-Peyret, C.: 4-D comparison method to study the NO_y partitioning in summer polar stratosphere – Influence of aerosol burden, Atmos. Chem. Phys., 5, 919–926, 2005.

Ferlemann, F., Camy-Peyret, C., Fitzenberger, R., Harder, H., Hawat, T., Osterkamp, H., Schneider, M., Perner, D., Platt, U., Vradelis, P., and Pfeilsticker, K.: Stratospheric BrO Profiles Measured at Different Latitudes and Seasons: Instrument Description, Spectral and Profile Retrieval, Geophys. Res. Lett., 25, 3847–3850, 1998.

Ferlemann, F., Bauer, N., Fitzenberger, R., Harder, H., Osterkamp, H., Perner, D., Platt, U., Schneider, M., Vradelis, P., and Pfeilsticker, K.: A new DOAS-instrument for stratospheric balloonborne trace gas studies, J. Appl. Opt., 39, 2377–2386, 2000.

Flittner, D., Bhartia, P., and Herman, B.: O_3 profiles retrieved from limb scatter measurements: Theory, Geophys. Res. Lett., 27, 2061–2064, 2000.

Frankenberg, C., Platt, U., and Wagner, T.: Iterative maximum a posteriori (IMAP)-DOAS for retrieval of strongly absorbing trace gases: Model studies for CH_4 and CO_2 retrieval from near infrared spectra of SCIAMACHY onboard Envisat, Atmos. Chem. Phys., 5, 9–22, 2005.

von Friedeburg, C.: Derivation of Trace Gas Information combining Differential Optical Absorption Spectroscopy with Radiative Transfer Modelling, PhD thesis, University of Heidelberg, Heidelberg, Germany, 2003.

von der Gathen, P., Rex, M., Harris, N. R. P., Lucic, D., Knudsen, B. M., Braathen, G. O., De Backer, H., Fabian, R., Fast, H., Gil, M., Kyrö, E., Mikkelsen, I. S., Rummukainen, M., Stähelin, J., and Varotsos, C.: Observational evidence for chemical ozone depletion over the Arctic in winter 1991–92, Nature, 375, 131–134, 1995.

Grainger, J. F. and Ring, J.: Anomalous Fraunhofer line profiles, Nature, 193, 762, 1962.

Greenblatt, G. D., Orlando, J. J., Burkholder, J. B., and Ravishankara, A. R.: Absorption measurements of oxygen between 330 and 1140 nm, J. Geophys. Res., 95, 18 577–18 582, 1990.

Haley, C. S., Brohede, S. M., Sioris, C. E., Griffioen, E., Murtagh, D. P., McDade, I. C., Eriksson, P., Llewellyn, E. J., Bazureau, A., and Goutail, F.: Retrieval of stratospheric O_3 and NO_2 profiles from Odin Optical Spectrograph and Infrared Imager System (OSIRIS) limb-scattered sunlight measurements, J. Geophys. Res., 109, D16303, doi:10.1029/2004JD004588, 2004.

Harder, H., Camy-Peyret, C., Ferlemann, F., Fitzenberger, R., Hawat, T., Osterkamp, H., Perner, D., Platt, U., Schneider, M., Vradelis, P., and Pfeilsticker, K.: Stratospheric BrO Profiles Measured at Different Latitudes and Seasons: Atmospheric Observations, Geophys. Res. Lett., 25, 3843–3846, 1998.

Harder, H., Bösch, H., Camy-Peyret, C., Chipperfield, M., Fitzenberger, R., Payan, S., Perner, D., Platt, U., Sinnhuber, B., and Pfeilsticker, K.: Comparison of measured and modeled stratospheric BrO: Implications for the total amount of stratospheric bromine, Geophys. Res. Lett., 27, 3695–3698, 2000.

Harder, J. W., Brault, J. W., Johnston, P., and Mount, G. H.: Temperature dependent NO_2 cross sections at high spectral resolution, J. Geophys. Res., 102, 3861–3879, 1997.

Hawat, T. M., Camy-Peyret, C., and Torguet, R. J.: Suntracker for atmospheric remote sensing, SPIE Optical Engineering, May 1998, 37(05), 1633–1642, 1998.

Hermans, C.: http://www.oma.be/BIRA-IASB/Scientific/Data/CrossSections/CrossSections.html, 2002.

Hendrick, F., Barret, B., Van Roozendael, M., Bösch, H., Butz, A., De Maziere, M., Goutail, F., Hermans, C., Lambert, J.-C., Pfeilsticker, K., and Pommereau, J.-P.: Retrieval of nitrogen dioxide stratospheric profiles from ground-based zenith-sky UV-visible observations: validation of the technique through correlative comparisons, Atmos. Chem. Phys., 4, 2091-2106, 2004.

Hoogen, R., Rozanov, V. V., and Burrows, J. P.: Ozone profiles from GOME satellite data: Algorithm description and first validation, J. Geophys. Res., 104, 8263–8280, 1999.

Kaiser, J. W. and Burrows, J. P.: Fast Weighting Functions for Retrievals from Limb Scattering Measurements, J. Quant. Spectrosc. Radiat. Transfer, 77(3), 273–283, 2003.

Kaiser, J. W., von Savigny, C., Eichmann, K.-U., Noël, S., Bovensmann, H., and Burrows, J. P.: Satellite Pointing Retrieval from Atmospheric Limb Scattering of Solar UV-B Radiation, Can. J. Phys., 82, 1041–1052, 2004.

Kerr, J. B., Evans, W. F. J., and McConnell, J. C.: The effects of NO_2 changes at twilight on tangent ray NO_2 measurements, Geophys. Res. Lett., 4, 577–579, 1977.

Krecl, P., Haley, C. S., Stegman, J., Brohede, S. M., and Berthet, A.: Retrieving the vertical distribution of stratospheric OClO from Odin/OSIRIS limb-scattered sunlight measurements, Atmos. Chem. Phys. Discuss., 5, 2989–3046, 2005.

Kühl, S.: Quantifying Stratospheric Chlorine Chemistry by the Satellite Spectrometers GOME and SCIAMACHY, PhD thesis, University of Heidelberg, Heidelberg, Germany, 2005.

Langematz, U., Labitzke, K., and Reimer, E.: Synoptic analysis and trajectories during the MAP/GLOBUS campaign 1983, Plan. Space Sci., 35, 5, 525–538, 1987.

Lary, D. J. and Pyle, J. A.: Diffuse radiation, twilight and photochemistry, J. Atmos. Chem., 13, 373-392, 1991.

Lu, C.-H., Yue, G. K., Manney, G. L., Jäger, H., and Mohnen, V. A.:

Lagrangian approach for Stratospheric Aerosol and Gas Experiment (SAGE) II intercomparisons, J. Geophys. Res., 105(D4), 4563–4572, doi:10.1029/1999JD901077, 2000.

Mauldin, L. E., Zaun, N. H., McCormick, M. P., Guy, J. J., and Vaughn, W. R.: Stratospheric Aerosol and Gas Experiment II Instrument: A Instrumental Description, Opt. Eng., 24, 307–312, 1985.

Mount, G. H., Rusch, D. W., Noxon, J. F., Zawodny, J. M., and Barth, C. A.: Measurements of stratospheric NO_2 from the SME satellite, J. Geophys. Res., 89, 1327-1340, 1984.

Orphal, J.: A critical review of the absorption cross-sections of O_3 and NO_2 in the ultraviolet and visible, J. Photochem. Photobiol. A: Chemistry, 157, 185-209, 2003.

Payan, S., Camy-Peyret, C., Lefèvre, F., Jeseck, P., Hawat, T., and Durry, G.: First direct simultaneous HCl and $ClONO_2$ profile measurements in the Arctic vortex, Geophys. Res. Lett., 25, 2663–2666, 1998.

Payan, S., Camy-Peyret, C., Jeseck, P., Hawat, T., Pirre, M., Renard, J.-B., Robert, C., Lefèvre, F., Kanzawa, H., and Sasano, Y.: Diurnal and nocturnal distribution of stratospheric NO_2 from solar and stellar occultation measurements in the Arctic vortex: comparison with models and ILAS satellite measurements, J. Geophys. Res., 104, 21 585–21 593, 1999.

Platt, U.: Differential optical absorption spectroscopy (DOAS), in: Air Monit. by Spectr. Techniques, edited by: Sigrist, M. W., Chemical Analysis Series, 127, 27–84, John Wiley & Sons, Inc., 1994.

Pfeilsticker, K., Erle, F., and Platt, U.: Observation of the stratospheric NO_2 latitudinal distribution in the northern winter hemisphere, J. Atmos. Chem., 32, 101–120, 1999.

Portmann, R. W., Brown, S. S., Gierczak, T., Talukdar, R. K., Burkholder, J. B., and Ravishankara, A. R.: Role of nitrogen oxides in the stratosphere: A reevaluation based on laboratory studies, Geophys. Res. Lett., 26, 2387-2390, 1999.

Reimer, E. and Kaupp, H.: Source indentification of odour compounds using trajectories, Proc. ECO-INFORMA 97, Eco-Informa Press, Bayreuth, 572-577, 1997.

Rodgers, C. D.: Inverse methods for atmospheric sounding, World Scientific, Singapore, New Jersey, London, Hongkong, 2000.

Rodgers, C. D. and Connor, J. B.: Intercomparison of remote sounding instruments, J. Geophys. Res., 108(D3), 4116, doi:10.1029/2002JD002299, 2003.

Roscoe, H. K. and Pyle, J. A.: Measurements of solar occultation – The error in a naive retrieval if the constituent's concentration changes, J. Atmos. Chem., 5, 323–341, 1987.

Rothman, L. S., Barbe, A., Chris Benner, D., Brown, L. R., Camy-Peyret, C., Carleer, M. R., Chance, K., Clerbaux, C., Dana, V., Devi, V. M., Fayt, A., Flaud, J.-M., Gamache, R. R., Goldman, A., Jacquemart, D., Jucks, K. W., Lafferty, W. J., Mandin, J.-Y., Massie, S. T., Nemtchinov, V., Newnham, D. A., Perrin, A., Rinsland, C. P., Schroeder, J., Smith, K. M., Smith, M. A. H., Tang, K., Toth, R. A., Vander Auwera, J., Varanasi, P., and Yoshino, K.: The HITRAN molecular spectroscopic database: edition of 2000 including updates through 2001, J. Quant. Spectrosc. Radiat. Transfer, 82, 5-44, 2003.

Rothman, L. S., Jacquemart, D., Barbe, A., Chris Benner, D., Birk, M., Brown, L. R., Carleer, M. R., Chackerian, C., Chance, K., Dana, V., Devi, V. M., Flaud, J.-M., Gamache, R. R., Goldman, A., Hartmann, J.-M., Jucks, K. W., Maki, A. G., Mandin, J.-Y., Massie, S. T., Orphal, J., Perrin, A., Rinsland, C. P., Smith, M. A. H., Tennyson, J., Tolchenov, R. N., Toth, R. A., Vander Auwera, J., Varanasi, P., and Wagner, G.: The HITRAN 2004 Molecular Spectroscopic Database, J. Quant. Spectrosc. Radiat. Transfer, 96, 139–204, 2005.

Rozanov, A.: Modeling of radiative transfer through a spherical planetary atmosphere: Application to atmospheric trace gases retrieval from occultation and limb-measurements in UV-Vis-NIR, Logos Verlag Berlin, Germany, 2001.

Rozanov A., Rozanov, V., Buchwitz, M., Kokhanovsky, A. and Burrows, J. P.: SCIATRAN 2.0 - A new radiative transfer model for geophysical applications in the 175-2400 nm spectral region, Adv. Space Res., 36, 5, 1015–1019, doi:10.1016/j.asr.2005.03.012, 2005a.

Rozanov, A., Bovensmann, H., Bracher, A., Hrechanyy, S., Rozanov, V. V., Sinnhuber, M., Stroh, F., and Burrows, J. P.: NO_2 and BrO vertical profile retrieval from SCIAMACHY limb measurements: Sensitivity studies, Adv. Space Res., 36, 5, 846–854, doi:10.1016/j.asr.2005.03.013, 2005b.

Rusch, D. W., Mount, G. H., Barth, C. A., Thomas, R. J., and Callan, M. T.: Solar mesosphere explorer ultraviolet spectrometer: measurements of ozone in the 1.0–0.1 mb region, J. Geophys. Res., 89, 11 677-11 678, 1984.

Russell III, J. M., Farmer, C. B., Rinsland, C. P., Zander, R., Froidevaux, L., Toon, G. C., Gao, B., Shaw, J., and Gunson, M. R.: Measurements of odd nitrogen compounds in the stratosphere by the ATMOS experiment on Spacelab 3, J. Geophys. Res., 93, 1718–1736, 1988.

Sander, S. P., Friedl, R. R., Ravishankara, A. R., Golden, D. M., Kolb, C. E., Kurylo, M. J., Huie, R. E., Orkin, V. L., Molina, M. J., Moortgat, G. K., and Finlayson-Pitts, B. J.: Chemical kinetics and photochemical data for use in atmoshperic studies; evaluation number 14, JPL-Publication 00-3, 2003.

Sasano, Y., Suzuki, M., and Yokota, T.: Stratospheric trace gas measurements with Improved limb Atmospheric Spectrometer (ILAS) for ADEOS satellite, Optics for protection of man and environment against natural and technological disasters, 43–48, 1993.

von Savigny, C., Haley, C. S., Sioris, C. E., McDade, I. C., Llewellyn, E. J., Degenstein, D., Evans, W. F. J., Gattinger, R. L., Griffioen, E., Kyrölä, E., Lloyd, N. D., McConnell, J. C., McLinden, C. A., Mégie, G., Murtagh, D. P., Solheim, B., and Strong, K.: Stratospheric Ozone Profiles retrieved from Limb Scattered Sunlight Radiance Spectra Measured by the OSIRIS Instrument on the Odin Satellite, Geophys. Res. Lett., 30, doi:10.1029/2002GL016401, 2003.

von Savigny, C., Kaiser, J. W., Bovensmann, H., Burrows, J. P., McDermid, I. S., and Leblanc, T.: Spatial and Temporal Characterization of SCIAMACHY Limb Pointing Errors During the First Three Years of the Mission, Atmos. Chem. Phys., 5, 2593–2602, 2005a.

von Savigny, C., McDade, I. C., Griffioen, E., Haley, C. S., Sioris, C. E., and Llewellyn, E. J.: Sensitivity studies and first validation of stratospheric ozone profile retrievals from Odin/OSIRIS observations of limb scattered solar radiations, Can. J. Phys., 83, 957–972, 2005b.

von Savigny, C., Rozanov, A., Bovensmann, H., Eichmann, K.-U., Noël, S., Rozanov, V. V., Sinnhuber, B.-M., Weber, M., and Burrows, J. P.: The ozone hole break-up in September 2002 as seen

by SCIAMACHY on Envisat, J. Atmos. Sci., 62(3), 721–734, 2005c.

Sierk, B., Richer, A., Rozanov, A., von Savigny, C, Schmoltner, A. M., Buchwitz, M., Bovensmann, H., and Burrows, J. P.: Retrieval and monitoring of atmospheric trace gas concentrations in nadir and limb geometry using the space-borne SCIAMACHY instrument, Environmental Monitoring and Assessment, in press, 2006.

Sioris, C. E., Haley, C. S., McLinden, C. A., von Savigny, C., McDade, I. C., McConnell, J. C., Evans, W. F. J., Lloyd, N. D., Llewellyn, E. L, Chance, K., Kurosu, T. P., Murtagh, D., Frisk, U., Pfeilsticker, K., Bösch, H., Weidner, F., Strong, K., Stegman, J., and Megie, G.: Stratospheric profiles of nitrogen dioxide observed by OSIRIS on the Odin satellite, J. Geophys. Res., 108, 4215, doi:10.1029/2002JD002672, 2003.

Sioris, C. E., Kurosu, T. P., Martin, R. V., and Chance, K.: Stratospheric and tropospheric NO_2 observed by SCIAMACHY: first results, Adv. Space Res., 34, 780–785, 2004.

Stutz, K. and Platt, U.: Numerical analysis and estimation of the statistical error of differential optical absorption spectroscopy measurements with least-square methods, Appl. Opt., 35, 30, 6041–6053, 1996.

Voigt, S., Orphal, J., and Burrows, J. P.: The Temperature- and Pressure-Dependence of the Absorption Cross-section of NO_2 in the 250–800 nm Region measured by Fourier-Transform Spectroscopy, J. Photochem. Photobiol. A, 149, 1–7, 2002.

Voigt, S., Orphal, J., Bogumil, K., and Burrows, J. P.: The Temperature dependence (203–293 K) of the absorption cross sections of O_3 in the 230–850 nm region measured by Fourier-transform spectroscopy, J. Photochem. Photobiol. A, 143, 1–9, 2001.

Weidner, F., Bösch, H., Bovensmann, H., Burrows, J. P., Butz, A., Camy-Peyret, C., Dorf, M., Gerilowski, K., Gurlit, W., Platt, U., von Friedeburg, C., Wagner, T., and Pfeilsticker, K.: Balloon-borne Limb profiling of UV/vis skylight radiances, O_3, NO_2, and BrO: Technical set-up and validation of the method, Atmos. Chem. Phys., 5, 1409–1422, 2005.